Article

Cell Host & Microbe

Host cells subdivide nutrient niches into discrete biogeographical microhabitats for gut microbes

Graphical abstract

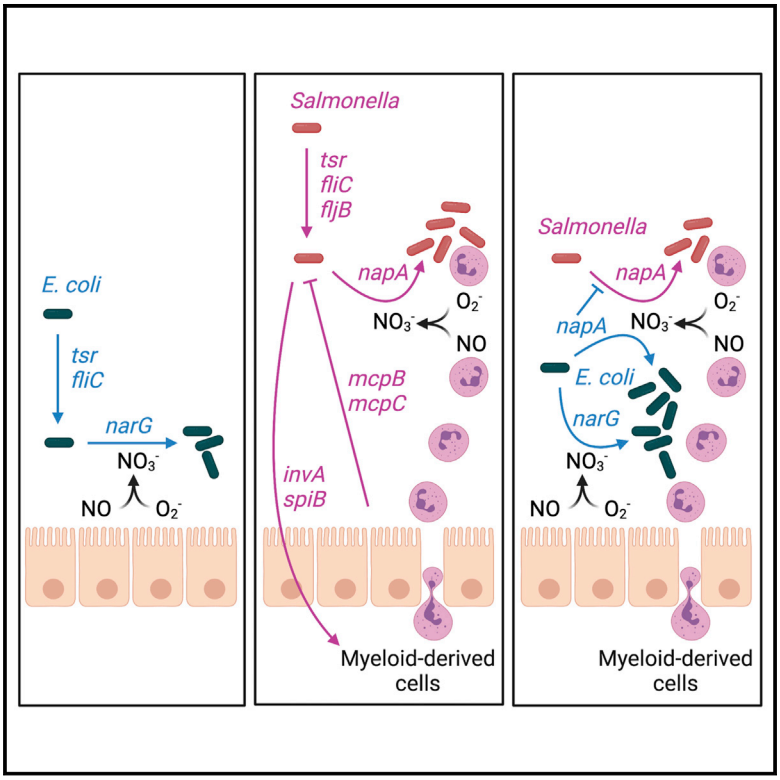

Highlights

- Commensal *Escherichia coli* utilizes epithelial-derived nitrate in the gut lumen
- *Salmonella* virulence factors attract phagocytes as main luminal nitrate sources
- *Salmonella* lacking virulence factors cannot access epithelial-derived nitrate
- Utilization of phagocyte-derived nitrate by *E. coli* checks *Salmonella* growth

Authors

Megan J. Liou, Brittany M. Miller, Yael Litvak, ..., Mariana X. Byndloss, Scott I. Simon, Andreas J. Bäumler

Correspondence

ajbaumler@ucdavis.edu

In brief

Liou et al. find that pathogenic *Salmonella* and commensal *E. coli* obtain nitrate, a critical resource, in distinct spatial microhabitats in the gut lumen, which are generated by different host-cell types. The ability of *E. coli* to invade the spatial microhabitat occupied by *Salmonella* contributes to colonization resistance.

Liou et al., 2022, Cell Host & Microbe *30*, 1–12
June 8, 2022
https://doi.org/10.1016/j.chom.2022.04.012

CellPress

Cell Host & Microbe

CellPress
OPEN ACCESS

Article

Host cells subdivide nutrient niches into discrete biogeographical microhabitats for gut microbes

Megan J. Liou,[1] Brittany M. Miller,[1] Yael Litvak,[2] Henry Nguyen,[1] Dean E. Natwick,[3] Hannah P. Savage,[1] Jordan A. Rixon,[4] Scott P. Mahan,[1] Hirotaka Hiyoshi,[5] Andrew W.L. Rogers,[1] Eric M. Velazquez,[1] Brian P. Butler,[6] Sean R. Collins,[3] Stephen J. McSorley,[4] Rasika M. Harshey,[7] Mariana X. Byndloss,[8] Scott I. Simon,[9] and Andreas J. Bäumler[1,10,*]

[1]Department of Medical Microbiology and Immunology, School of Medicine, University of California at Davis, One Shields Ave, Davis, CA 95616, USA

[2]Department of Biological Chemistry, The Alexander Silberman Institute of Life Sciences, The Hebrew University of Jerusalem, Edmond J. Safra Campus Givat-Ram, Jerusalem 9190401, Israel

[3]Department of Microbiology and Molecular Genetics, College of Biological Sciences, University of California at Davis, One Shields Ave, Davis, CA 95616, USA

[4]Center for Immunology and Infectious Diseases and Department of Anatomy, Physiology and Cell Biology, School of Veterinary Medicine, University of California at Davis, One Shields Ave, Davis, CA 95616, USA

[5]Department of Bacteriology, Institute of Tropical Medicine, Nagasaki University, 1-12-4 Sakamoto, Nagasaki 852-8523, Japan

[6]Department of Pathobiology, School of Veterinary Medicine, St. George's University, Grenada, West Indies

[7]Department of Molecular Biosciences and LaMontagne Center for Infectious Diseases, The University of Texas at Austin, Austin, TX 78712, USA

[8]Vanderbilt Institute for Infection, Immunology and Inflammation and Department of Pathology, Microbiology, and Immunology, Vanderbilt University Medical Center, Nashville, TN 37232, USA

[9]Department of Biomedical Engineering, College of Engineering and Department of Dermatology, School of Medicine, University of California at Davis, One Shields Ave, Davis, CA 95616, USA

[10]Lead contact

*Correspondence: ajbaumler@ucdavis.edu

https://doi.org/10.1016/j.chom.2022.04.012

SUMMARY

Changes in the microbiota composition are associated with many human diseases, but factors that govern strain abundance remain poorly defined. We show that a commensal *Escherichia coli* strain and a pathogenic *Salmonella enterica* serovar Typhimurium isolate both utilize nitrate for intestinal growth, but each accesses this resource in a distinct biogeographical niche. Commensal *E. coli* utilizes epithelial-derived nitrate, whereas nitrate in the niche occupied by *S.* Typhimurium is derived from phagocytic infiltrates. Surprisingly, avirulent *S.* Typhimurium was shown to be unable to utilize epithelial-derived nitrate because its chemotaxis receptors McpB and McpC exclude the pathogen from the niche occupied by *E. coli*. In contrast, *E. coli* invades the niche constructed by *S.* Typhimurium virulence factors and confers colonization resistance by competing for nitrate. Thus, nutrient niches are not defined solely by critical resources, but they can be further subdivided biogeographically within the host into distinct microhabitats, thereby generating new niche opportunities for distinct bacterial species.

INTRODUCTION

The colon harbors the largest microbial community in the human body, containing more than one hundred bacterial species (Human Microbiome Project, 2012; Qin et al., 2010) that are stably maintained for months (David et al., 2014). For these bacterial species to co-exist, each member within the microbial community has to utilize some critical resources better than any of the other coexisting species, and the abundance of these critical resources determines the abundance of the microbe occupying the corresponding nutrient niches (Freter et al., 1983). The co-existence of more than 100 bacterial species consequently suggests that the colonic habitat comprises more than 100 discrete nutrient niches, but their characteristics remain poorly defined (Freter et al., 1983; Qin et al., 2010). A better understanding of how diet and host environment carve out each available nutrient niche will be critical for fully comprehending microbiota assembly and function.

In the large intestine, dietary fiber is one of the critical resources with the greatest abundance, making fermentation of fiber one of the most successful metabolic traits in this habitat patch. As a result, the colonic microbiota is dominated by members of the classes *Clostridia* (phylum *Firmicutes*) and *Bacteroidia* (phylum *Bacteroidetes*) (Human Microbiome Project, 2012), two taxa that encode a broad spectrum of carbohydrate-active enzymes (Kaoutari et al., 2013). While the role of dietary fiber in maintaining dominant bacterial taxa within the gut microbiota is a subject of intense investigation,

comparatively little is known about the nutrient niches occupied by minority species.

In addition to diet-derived factors that shape the environment inhabited by the microbiota, the host generates microhabitats through the release of antimicrobials or by providing critical resources that sculpt microbial growth. Members of the *Enterobacterales* (*ord. nov.* [Adeolu et al., 2016]) are minority species within the gut microbiota of mammals (Ley et al., 2008), which utilize critical resources provided by the host. In the nutrient niche they occupy in the large intestine, commensal *Enterobacterales* oxidize organic compounds using host-derived respiratory electron acceptors, including nitrate (Jones et al., 2007; Jones et al., 2011). Nitrate is an inert end product of the host's nitric oxide metabolism, which depends on the synthesis of the host enzyme inducible nitric oxide synthase (iNOS) in the gut (reviewed in the study conducted by Winter et al., 2013a). During homeostasis, the scarcity of nitrate and other respiratory electron acceptors is one of the reasons why commensal members of the *Enterobacterales*, such as *Escherichia coli*, are present in low abundance within the microbiota (Byndloss et al., 2017). In contrast, intestinal inflammation triggered by pathogenic members of the *Enterobacterales*, such as *Salmonella enterica* serovar (*S*. Typhimurium), increases the luminal availability of host-derived respiratory electron acceptors, including nitrate, which drives a pathogen expansion within the gut microbiota (Lopez et al., 2015, 2012; Rivera-Chávez et al., 2016b; Winter et al., 2010). Similarly, conditions of noninfectious intestinal inflammation, such as inflammatory bowel disease in humans or chemically induced colitis in mice, increases the availability of host-derived nitrate in the intestinal lumen, which in turn drives an expansion of commensal *E. coli* within the gut microbiota (Winter et al., 2013b; Zhu et al., 2018). These data suggest that host-derived nitrate is a critical resource that defines the nutrient niche occupied by *Enterobacterales* and that the abundance of this critical resource determines the abundance of this taxon within the gut microbiota.

The main virulence factors required for inducing intestinal inflammation are two Type III secretion systems encoded by *Salmonella* pathogenicity islands—1 (T3SS-1) and 2 (T3SS-2), respectively (Barthel et al., 2003; Hapfelmeier et al., 2005; Matsuda et al., 2019; Tsolis et al., 1999; Zhang et al., 2002). The ability to use these virulence factors to increase the availability of critical host-derived resources is a property that distinguishes *S.* Typhimurium from commensal species, such as *E. coli* (Gillis et al., 2018; Lopez et al., 2015, 2012; Rivera-Chávez et al., 2016b; Winter et al., 2010). It is therefore tempting to speculate that an avirulent *S.* Typhimurium mutant that lacks functional T3SS-1 and T3SS-2 would occupy the same nutrient niche in the gut lumen as commensal *E. coli*, because both species utilize the same critical resource, nitrate. However, this prediction rests on data from population averages, whereas the microhabitats occupied by these two closely related microorganisms in the gut lumen or in the colonic mucus layers remain poorly characterized. Here we combined microscopy with bacterial and host genetics to provide a deeper understanding of the nutrient niches occupied by closely related members of the *Enterobacterales* in the gut ecosystem. By illuminating the biogeography of *Enterobacterales* populations in the large intestine, this approach revealed how the host generates niche opportunities for closely related microorganisms by sculpting discrete spatial microhabitats.

RESULTS

Biogeographical features distinguish the niches occupied by *S.* Typhimurium 14028 and *E. coli* Nissle 1917

To investigate whether virulence factors are the sole source of ecological diversification among closely related *Enterobacterales*, we determined whether the inactivation of T3SS-1 and T3SS-2 by mutations in *invA* and *spiB*, respectively, would result in an avirulent *S.* Typhimurium strain that occupies an ecological position similar to commensal *E. coli*. To this end, we compared the commensal *E. coli* strain Nissle 1917 (Nissle, 1925), a human isolate that is marketed as a probiotic, with derivatives of *S.* Typhimurium strain ATCC14028 that were either fully virulent (wild type) or avirulent (*invA spiB* mutant) (Table S1). *E. coli* strain Nissle 1917 is similar in its ability to confer colonization resistance against *S.* Typhimurium infection in mice as murine commensal *E. coli* isolates (Velazquez et al., 2019). To ensure engraftment of *E. coli* and *S.* Typhimurium strains at levels high enough for detection by fluorescence microscopy, mice were pretreated with a single dose of streptomycin, an antibiotic commonly used to study intestinal colonization by these species in the mouse model (Barthel et al., 2003; Hapfelmeier et al., 2005; Jones et al., 2007, 2011). Infection with wild-type *S.* Typhimurium triggers migration of phagocytes into the intestinal lumen, which was visualized in mice expressing the gene encoding enhanced green fluorescent protein (*EGFP*) under control of the lysozyme M (*LysM*) promoter (*lys-EGFP-ki* mice), in which phagocytes belonging to the granulocyte, monocyte, and macrophage lineages are green fluorescent (Faust et al., 2000). Infection with the *S.* Typhimurium wild type resulted in marked accumulation of green fluorescent phagocytes in the intestinal lumen, where they were found in close association with the pathogen (Figure 1A), which was consistent with a previous report (Loetscher et al., 2012). In contrast, no fluorescent phagocytes were detected in the intestinal lumen of mice infected with the *S.* Typhimurium *invA spiB* mutant (Figure 1B) or mice inoculated with sterile medium (mock infection) (Figure 1C). These data suggested that whereas phagocytes recruited to the intestinal lumen during infection with the *S.* Typhimurium wild type visibly remodeled the intestinal environment, the *invA spiB* mutant encountered a habitat that more closely resembled that encountered in mock-infected mice, suggesting the latter might occupy a niche similar to commensal *E. coli*.

To test this idea, we compared the localization of the avirulent *S.* Typhimurium *invA spiB* mutant with that of commensal *E. coli* in the colon of streptomycin-pretreated C57BL/6 mice (Figure 1D). We used immunofluorescence to determine the distribution of bacteria within the intestinal lumen by segmenting images (Figure 1E) and measuring distances from representative bacterial "seed pixels" to the actin brush border of the epithelium (Figure 1F). We found that *E. coli* was concentrated close to the brush border (Figure 1F), whereas the *S.* Typhimurium *invA spiB* mutant had a much broader distribution (Figure 1G). We quantified this difference by computing the interquartile range of distances for each strain and found a significant difference

Please cite this article in press as: Liou et al., Host cells subdivide nutrient niches into discrete biogeographical microhabitats for gut microbes, Cell Host & Microbe (2022), https://doi.org/10.1016/j.chom.2022.04.012

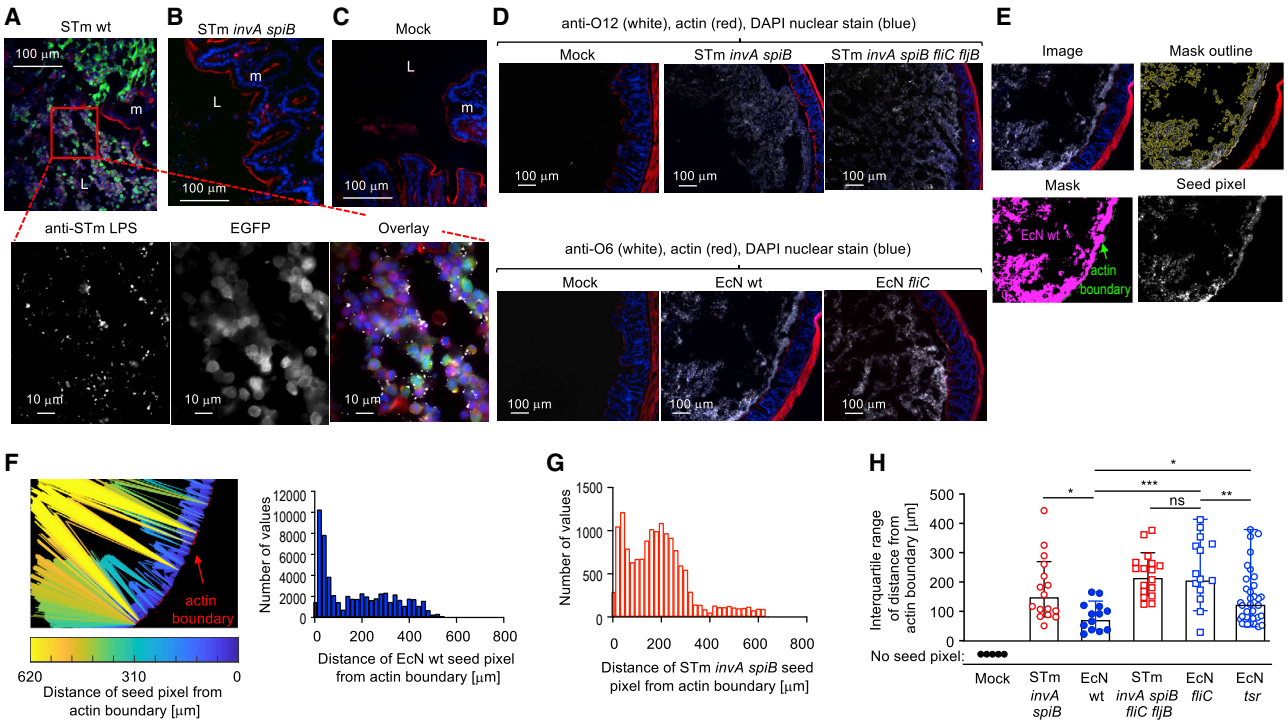

Figure 1. Visualization of microhabitats occupied by *E. coli* and *S.* Typhimurium in the colon of streptomycin-pretreated mice

(A–C) Groups of streptomycin-pretreated *lys-EGFP-ki* mice (N = 4) were infected with the *S.* Typhimurium wild type (STm WT) (A), an avirulent *invA spiB* mutant (STm *invA spiB*) (B), or mock infected (Mock) (C). Sections of the cecum were stained for EGFP (green fluorescence), the O12-antigen of *S.* Typhimurium lipopolysaccharide (LPS) (white fluorescence), actin (red fluorescence), and DAPI nuclear stain (blue fluorescence). (A) The red rectangle in the top panel indicates an area that is shown at higher magnification in the three bottom panels, which show staining for *S.* Typhimurium LPS (anti-STm LPS; left panel), EGFP synthesis in phagocytes (EGFP; middle panel) and an overlay (right panel).

(D–G) Groups of streptomycin-pretreated C57BL/6 mice (*N* is indicated in G) were mock infected (Mock) or infected with an avirulent *S.* Typhimurium *invA spiB* mutant (STm *invA spiB*), a nonmotile avirulent *S.* Typhimurium *invA spiB fliC fljB* mutant (STm *invA spiB fliC fljB*), *E. coli* Nissle 1917 (EcN WT), or a nonmotile *E. coli* Nissle 1917 *fliC* mutant (EcN *fliC*).

(D) Sections of the colon were stained for actin (red fluorescence), DAPI nuclear stain (blue fluorescence), and either the O12-antigen of *S.* Typhimurium LPS (white fluorescence, top panels) or the O6-antigen of *E. coli* Nissle 1917 LPS (white fluorescence, bottom panels).

(E–G) Quantification of bacterial distance from epithelium.

(E) Example of quantitative analysis of an immunofluorescence image (top left panel) by segmenting the actin brush border (actin boundary) and bacterial colonization zones (top right panel), removing background outside the masked areas (bottom left panel) and generating seed pixels within colonization zones to represent bacterial positions (bottom right panel).

(F) Lines connecting each seed pixel with the closest pixel within the actin boundary (left panel) are colored to indicate their lengths according to the color scheme shown below. The graph on the right plots the number of lines (values) against their lengths for a section from a mouse infected with *E. coli* Nissle 1917 (EcN WT).

(G) The graph plots the number of lines (values) against their lengths for a section from a mouse infected with an avirulent *S.* Typhimurium *invA spiB* mutant (STm *invA spiB*).

(H) The graph shows the average interquartile range of distances from the actin boundary for the indicated bacterial strains (bars). Each symbol (dots/squares) represents data from one microscopic image. *p < 0.05; ***p < 0.001; ns, p > 0.05.

(Figure 1H), suggesting that each strain might occupy a distinct spatial habitat in the gut lumen.

To determine whether this difference in the spatial distribution of bacteria required motility, the experiment was repeated after mutating genes encoding flagellin, the major protein subunit of flagella, in *E. coli* (*fliC* mutant) and avirulent *S.* Typhimurium (*invA spiB fliC fljB* mutant). Interestingly, a nonflagellated *E. coli* strain colonized the colon at a significantly increased interquartile range of distance from the actin brush border, producing a similar spatial distribution as observed for the nonflagellated avirulent *S.* Typhimurium strain (Figures 1D and 1H). The dependence of *E. coli* localization on flagella-based motility suggested that its nutrient niche involved a spatial component.

Genetic evidence suggests that nitrate is available in two distinct nutrient niches

Spatial information from microscopic analysis (Figure 1H) raised the question as to whether its localization in closer proximity to the epithelial brush border provided commensal *E. coli* access to a nutrient niche that differed from the one occupied by avirulent *S.* Typhimurium (*invA spiB* mutant). Flagella-based motility enables *E. coli* to seek out environments rich in respiratory electron acceptors, such as nitrate, through a process termed energy taxis (Greer-Phillips et al., 2003; Rebbapragada et al., 1997). We thus investigated whether the fitness advantage conferred by nitrate respiration during growth of *E. coli* in the colons of streptomycin-pretreated mice (Spees et al., 2013) was dependent on

Please cite this article in press as: Liou et al., Host cells subdivide nutrient niches into discrete biogeographical microhabitats for gut microbes, Cell Host & Microbe (2022), https://doi.org/10.1016/j.chom.2022.04.012

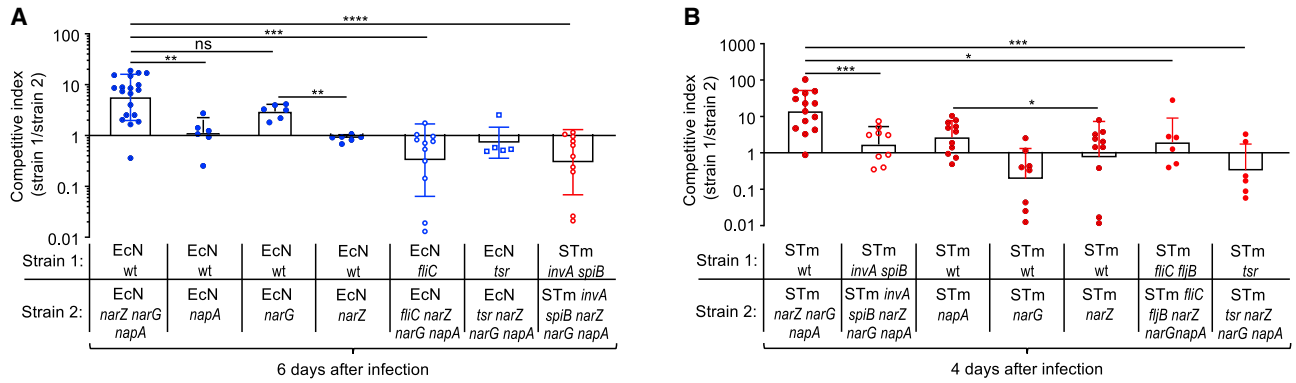

Figure 2. *E. coli* and *S.* Typhimurium use motility and energy taxis to access nitrate in distinct microhabitats

(A and B) Groups of streptomycin-pretreated C57BL/6 mice (*N* is indicated by the number of dots) were infected with the indicated mixtures of *E. coli* Nissle 1917 (EcN) or *S.* Typhimurium (STm) strains and colon contents collected 6 days after infection (A) or 4 days after infection (B) to determine the competitive index. Bars represent geometric mean ± geometric error. *p < 0.05; **p < 0.01; ***p < 0.001; ****p < 0.0001; ns, p ≥ 0.05.

motility and energy taxis. Genetic ablation of nitrate respiration through mutations in the nitrate reductase genes *narZ*, *narG*, and *napA* reduced fitness of *E. coli*, as indicated by reduced recovery of the *narA narG napA* mutant compared with the wild type from streptomycin-pretreated mice inoculated with a 1:1 mixture of both strains (Figure 2A). *E. coli* used mainly nitrate reductase A encoded by the *narGHI* genes for nitrate respiration in its nutrient niche, as revealed by comparing the fitness of the wild type with mutants lacking either *narZ*, *narG*, or *napA*. This fitness advantage conferred by nitrate respiration required motility, because it was no longer observed when we compared fitness of a nonmotile strain (*E. coli fliC* mutant) with that of a nonmotile nitrate-respiration-deficient strain (*E. coli fliC narZ narG napA* mutant). Similarly, genetic ablation of *tsr*, the gene encoding the energy taxis receptor for nitrate (Rivera-Chávez et al., 2013), abrogated the fitness advantage conferred by nitrate respiration in *E. coli* (Figure 2A). Furthermore, an *E. coli tsr* mutant colonized the colon at a significantly increased interquartile range of distance from the actin brush border compared with *E. coli* wild type (Figure 1G). Notably, similar numbers of an avirulent *S.* Typhimrium (*invA spiB*) mutant and an avirulent nitrate-respiration-deficient *S.* Typhimurium (*invA spiB narZ narG napA*) mutant were recovered from mice inoculated with a 1:1 mixture of both strains (Figure 2A). These results provided genetic evidence that the nutrient niches occupied by *E. coli* and avirulent *S.* Typhimurium differed, because only the former resided in a habitat that provided access to nitrate.

Interestingly, previous reports suggest that nitrate respiration provides a growth benefit for virulent wild-type *S.* Typhimurium in the large intestine (Lopez et al., 2015, 2012; McLaughlin et al., 2019), suggesting that colitis generates a nutrient niche in which the pathogen has access to nitrate. Consistent with these reports, the *S.* Typhimurium wild type was recovered in higher numbers than a nitrate-respiration-deficient strain (*narZ narG napA* mutant) when streptomycin-pretreated mice were inoculated with a 1:1 mixture of both strains (Figure 2B). In contrast to *E. coli* (Figure 2A), *S.* Typhimurium used mainly the periplasmic nitrate reductase NapA for nitrate respiration in its nutrient niche, as revealed by comparing the fitness of the wild type with mutants lacking either *narZ*, *narG*, or *napA* (Figure 2B). The fitness advantage conferred by nitrate respiration required motility, because it was no longer observed when we compared fitness of a nonmotile strain (*S.* Typhimurium *fliC fliB* mutant) with that of a nonmotile nitrate-respiration-deficient strain (*S.* Typhimurium *fliC fliB narZ narG napA* mutant). Similarly, genetic ablation of energy taxis toward nitrate by inactivation of *tsr* abrogated the fitness advantage conferred by nitrate respiration in virulent *S.* Typhimurium (*S.* Typhimurium *tsr* versus *S.* Typhimurium *tsr narZ narG napA* mutant) (Figure 2B). However, unlike *E. coli*, avirulent *S.* Typhimurium was not able to access host-derived nitrate in the absence of intestinal inflammation, as indicated by equal recovery of an avirulent *S*. Typhimrium (*invA spiB*) mutant and an avirulent nitrate-respiration-deficient *S.* Typhimurium (*invA spiB narZ narG napA*) mutant from streptomycin-pretreated mice inoculated with a 1:1 mixture of both strains (Figure 2B). Collectively, these data suggested that the nitrate-containing nutrient niche constructed by *S.* Typhimurium virulence factors was distinct from the nitrate-containing nutrient niche occupied by *E. coli* Nissle 1917.

Virulence factors construct a nutrient niche containing phagocyte-derived nitrate

To further characterize the nutrient niche inhabited by *S.* Typhimurium, streptomycin-pretreated mice were mock infected or infected with the *S.* Typhimurium wild type, a *S.* Typhimurium *invA spiB* mutant, or *E. coli*. Inflammatory lesions in histological sections of the colon (Figure 3A), elevated expression of proinflammatory genes in the cecal mucosa (Figure 3B) and a robust increase in the concentration of nitrate in cecal mucus (Figure 3C) were only observed after infection with virulent wild-type *S.* Typhimurium, but not in mice inoculated with an avirulent *S.* Typhimurium strain (*invA spiB* mutant), with commensal *E. coli*, or with sterile medium (mock infection). Furthermore, only infection with virulent *S.* Typhimurium (wild type) triggered an obvious increase in the concentration of the granulocyte marker myeloperoxidase (MPO) in cecal contents (Figure 3D), thus corroborating the striking remodeling of the luminal environment by phagocytes observed by microscopic analysis (Figure 1A).

Based on these observations we postulated that both wild-type *S.* Typhimurium and *E. coli* use motility and chemotaxis to

Please cite this article in press as: Liou et al., Host cells subdivide nutrient niches into discrete biogeographical microhabitats for gut microbes, Cell Host & Microbe (2022), https://doi.org/10.1016/j.chom.2022.04.012

CellPress
OPEN ACCESS

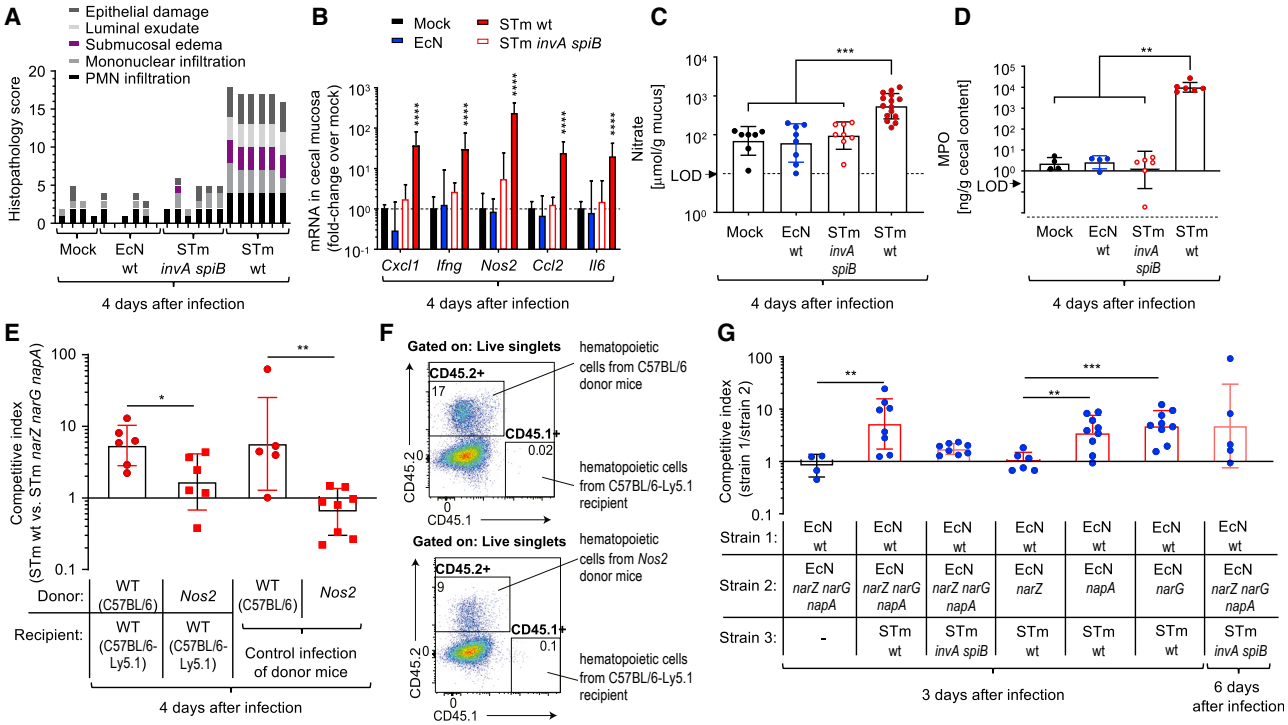

Figure 3. Phagocyte-derived nitrate constructs a nutrient niche for *S.* Typhimurium that can also be accessed by commensal *E. coli*

(A–D) Groups of streptomycin-pretreated C57BL/6J mice were mock infected (Mock) or infected with *E. coli* Nissle 1917 (EcN WT), avirulent *S.* Typhimurium (STm *invA spiB*), or virulent *S.* Typhimurium (STm WT) and organs collected 4 days after infection.

(A) Histological sections of the cecum were blinded and scored for lesions by a veterinary pathologist. Each bar represents data from one animal.

(B) Transcript levels of the indicated proinflammatory genes were determined by quantitative real-time PCR in RNA isolated from the cecal mucosa.

(C) Nitrate concentrations in cecal mucus scrapings determined by a modified Griess assay.

(D) Levels of myeloperoxidase in cecal contents was determined by ELISA.

(C and D) Each dot represents data from one animal.

(E and F) Lethally irradiated C57BL6/J-Ly5.1 mice received a bone-marrow transplant from wild-type (WT) C57BL/6 donor mice or *Nos2*-deficient donor mice. The resulting groups of bone-marrow chimera mice along with groups of C57BL/6- and *Nos2*-deficient donor mice were pretreated with streptomycin and then infected with the indicated mixtures of *S.* Typhimurium strains.

(E) Competitive index of *S.* Typhimurium strains recovered from colon contents. Bars represent geometric mean ± geometric error.

(F) Representative images showing flow cytometric analysis of intestinal cells from bone-marrow chimera mice to distinguish hematopoietic cells of the recipient ($CD45.1^+$) from hematopoietic cells of the C57BL/6- (top panel) or *Nos2*-deficient (bottom panel) donor ($CD45.2^+$).

(G) Groups of streptomycin-pretreated C57BL/6 mice (N is indicated by the number of dots) were infected with the indicated *S.* Typhimurium (STm) strains, followed by inoculation with *E. coli* (EcN) strain mixtures. Bars represent geometric mean ± geometric error. *$p < 0.05$; **$p < 0.01$; ***$p < 0.001$; ****$p < 0.0001$; ns, $p > 0.05$.

reach a microhabitat in which their growth is fueled by nitrate respiration (Figures 2A and 2B). However, although nitrate is a critical resource for growth of both bacterial species, their respective nutrient niches represent physically distinct microhabitats in the gut lumen. We further hypothesized that the microhabitat occupied by wild-type *S.* Typhimurium is constructed by phagocytes that migrate into the intestinal lumen (Figure 1A), and that an exclusive reliance on a phagocyte-derived nutrient niche for accessing nitrate explains why the avirulent *S.* Typhimurium *invA spiB* mutant can no longer access this critical resource in the gut (Figures 2A and 2B). Generation of host-derived nitrate requires *Nos2*, a gene encoding iNOS (Lopez et al., 2012; Spees et al., 2013; Winter et al., 2013b). Consistent with previous reports (Lopez et al., 2015, 2012), a nitrate-respiration-dependent fitness advantage was no longer observed in *Nos2*-deficient mice infected with a 1:1 mixture of the *S.* Typhimurium wild type and a *narZ narG napA* mutant (Figure 3E), suggesting that production of host-derived nitrate required an intact *Nos2* gene. However, nitrate can be derived from different host-cell types expressing *Nos2*, such as epithelial cells (Byndloss et al., 2017) or phagocytes (McLaughlin et al., 2019). To test our hypothesis, we wanted to generate mice that lack *Nos2* expression in phagocytes but have intact *Nos2* expression in the intestinal epithelium. To this end we generated bone-marrow chimera mice through transfer of hematopoietic cells from CD45.2-positive donor mice (*Nos2*-deficient mice or C57BL/6 mice) into lethally irradiated recipient mice that were positive for CD45.1 (C57BL/6-Ly5.1 mice). Allelic variants of leukocyte common antigen CD45 (i.e., CD45.1 and CD45.2) can be differentiated by flow cytometry, which confirmed successful engraftment of hematopoietic cells from the respective donor mice in each of the recipient mice (Figures 3F, S1, and S2A). C57BL/6-Ly5.1 mice that received a bone-marrow transplant from *Nos2*-deficient mice have somatic cells (e.g.,

intestinal epithelial cells) that contain an intact *Nos2* gene, whereas their hematopoietic cells (e.g., phagocytes) are *Nos2*-deficient. A fitness advantage of the *S.* Typhimurium wild type over a *narZ narG napA* mutant was observed in the colon contents of C57BL/6-Ly5.1 mice that received a bone-marrow transplant from C57BL/6 mice, but not in C57BL/6-Ly5.1 mice that received a bone-marrow transplant from *Nos2*-deficient mice (Figure 3E). In contrast, nitrate respiration did not provide a fitness advantage in the spleens of donor mice or bone-marrow chimera mice (Figure S2B). These data supported our hypothesis that nitrate available in the nutrient niche occupied by wild-type *S.* Typhimurium in the intestinal lumen required *Nos2* expression in hematopoietic cells, whereas *Nos2* expression in somatic cells was not sufficient.

Next, we wanted to investigate whether commensal *E. coli* could invade the nutrient niche that is constructed by *S.* Typhimurium-induced inflammation (Figure 1A). Whereas a nitrate-respiration-dependent fitness advantage was observed for *E. coli* in streptomycin-pretreated mice 6 days after infection (Figure 2A), this phenotype did not manifest at earlier time points (i.e., 3 days) after infection (Figure 3G). However, when *E. coli* strains (wild type and *narZ narG napA* mutant) were co-administered together with wild-type *S.* Typhimurium, the *E. coli* wild type was recovered in significantly higher numbers than the *E. coli narZ narG napA* mutant already at 3 days after infection. These data suggested that *S.* Typhimurium-induced intestinal inflammation constructed a new nutrient niche that enabled *E. coli* to access nitrate even at very early time points after infection. In line with this hypothesis, nitrate respiration of *E. coli* early after coinfection required *S.* Typhimurium virulence factors, because it was no longer observed 3 days after co-administrations of *E. coli* strains with an *S.* Typhimurium *invA spiB* mutant. We then investigated whether *napA*, which was used by *S.* Typhimurium for nitrate respiration (Figure 2B), could serve as a genetic marker for the nutrient niche constructed by virulence factors of the pathogen. This idea would predict that *E. coli*, which uses *narG* for nitrate respiration in the healthy gut (Figure 2A), would require *napA* for nitrate respiration once it invades the nutrient niche constructed by *S.* Typhimurium virulence factors. Consistent with this prediction, during coinfection with the *S.* Typhimurium wild type, *E. coli* required both *napA* and *narG* for nitrate respiration, as suggested by comparing the fitness of the *E. coli* wild type with *E. coli* mutants lacking either *narZ*, *narG*, or *napA* (Figure 3G).

To investigate whether *E. coli* relocalizes to a phagocyte rich space generated by *S.* Typhimurium virulence factors (Figure 1A), we used immunofluorescence microscopy. Coinfection of streptomycin-treated *lys-EGFP-ki* mice with the *S.* Typhimurium wild type resulted recruitment of phagocytes in the intestinal lumen, and *E. coli* was found in close association with these host cells in the cecal lumen (Figure S3A). We then quantified the localization of *E. coli* by computing the interquartile range of distances from the brush border. In streptomycin-treated mice inoculated with *E. coli* alone, the commensal was concentrated close to the brush border, whereas during *S*. Typhimurium coinfection *E. coli* had a broader distribution (Figure S3B), thus further supporting the idea that the commensal invaded a spatial niche generated by the pathogen.

Collectively, these data support the idea that *S.* Typhimurium virulence factors construct a nutrient niche in which both the pathogen and commensal *E. coli* can access phagocyte-derived nitrate.

Commensal *E. coli* access epithelial-derived nitrate in their nutrient niche

Whereas the data above suggest that phagocyte-derived nitrate was a marker of the nutrient niche occupied by virulent *S.* Typhimurium, phagocytes are commonly absent from the intestinal habitat encountered by commensal *E. coli*. Previous work shows that luminal nitrate in streptomycin-treated mice is attributable to epithelial *Nos2* expression (Byndloss et al., 2017). We therefore wanted to determine whether commensal *E. coli* occupy a niche in which they can access epithelial-derived nitrate. Streptomycin pretreatment has recently been shown to induce *Nos2* expression in the intestinal epithelium by decreasing signaling through the peroxisome proliferator-activated receptor gamma (PPAR-γ), which is a negative regulator of the *Nos2* gene (Byndloss et al., 2017). To generate two lines of mice that differed specifically with regard to epithelial *Nos2* expression, we bred mice lacking PPAR-γ in the intestinal epithelium (*Pparg*$^{fl/fl}$*Villin*$^{cre/-}$ mice) and wild-type littermate control animals (*Pparg*$^{fl/fl}$*Villin*$^{-/-}$ mice). Experiments using these mice were performed without streptomycin pretreatment.

Consistent with a previous report (Byndloss et al., 2017), detection of *Nos2* transcripts in RNA isolated from preparations of colonic epithelial cells revealed increased *Nos2* expression in mice lacking PPAR-γ in the intestinal epithelium (*Pparg*$^{fl/fl}$*Villin*$^{cre/-}$ mice) compared with littermate control animals (*Pparg*$^{fl/fl}$*Villin*$^{-/-}$mice) (Figure 4A). Furthermore, the nitrate concentration in cecal mucus scrapings was elevated in mice lacking PPAR-γ in the intestinal epithelium (*Pparg*$^{fl/fl}$*Villin*$^{cre/-}$ mice) compared with littermate control animals (*Pparg*$^{fl/fl}$*Villin*$^{-/-}$ mice) (Figure 4B). Inoculation of mice with a 1:1 mixture of the *E. coli* wild type and an isogenic *narZ narG napA* mutant revealed that genetic ablation of nitrate respiration reduced fitness in mice lacking PPAR-γ in the intestinal epithelium (*Pparg*$^{fl/fl}$*Villin*$^{cre/-}$ mice), but not in littermate control animals (*Pparg*$^{fl/fl}$*Villin*$^{-/-}$ mice) (Figure 4C). These data supported the idea that, in the absence of intestinal inflammation (Figure 4D), nitrate available in the nutrient niche occupied by *E. coli* was derived from the intestinal epithelium. Interestingly, avirulent *S.* Typhimurium was unable to access this source of nitrate, as indicated by equal recovery of nitrate respiration proficient (*S.* Typhimurium *invA spiB* mutant) and nitrate-respiration-deficient (*S.* Typhimurium *invA spiB narZ narG napA* mutant) bacteria from mice lacking PPAR-γ in the intestinal epithelium (*Pparg*$^{fl/fl}$*Villin*$^{cre/-}$ mice) (Figure 4C). These data further support the idea that, in the absence of intestinal inflammation, avirulent *S.* Typhimurium strains did not have access to the nutrient niche that is occupied by commensal *E. coli*.

The chemotaxis receptors McpB and McpC exclude *S.* Typhimurium from a nutrient-niche containing epithelial-derived nitrate

Next, we wanted to obtain mechanistic insights into why avirulent *S.* Typhimurium was unable to enter the nutrient niche occupied by commensal *E. coli*. Since localization of commensal

Please cite this article in press as: Liou et al., Host cells subdivide nutrient niches into discrete biogeographical microhabitats for gut microbes, Cell Host & Microbe (2022), https://doi.org/10.1016/j.chom.2022.04.012

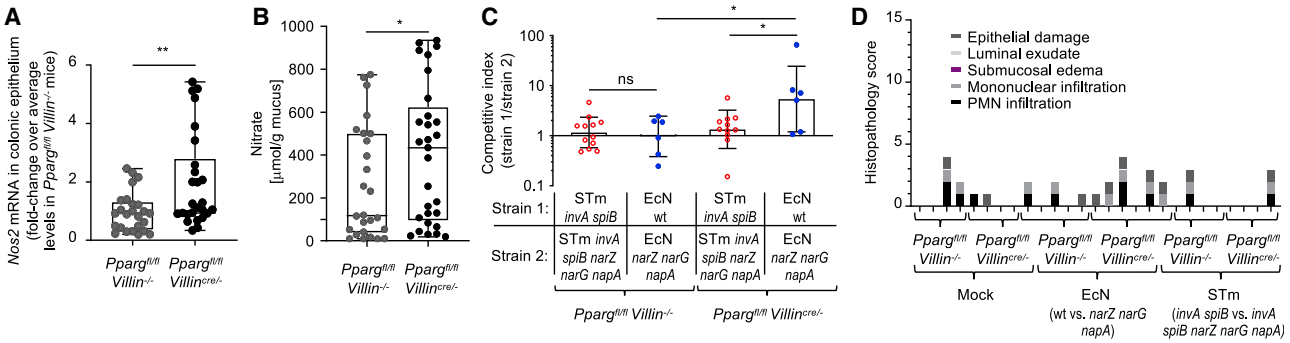

Figure 4. Epithelial-derived nitrate constructs a nutrient niche for *E. coli* that cannot be accessed by avirulent *S.* Typhimurium

(A and B) The colonic epithelium (A) or cecal mucus (B) were collected from groups of mice (*N* is indicated by the number of dots) lacking expression of *Pparg* in the intestinal epithelium (*Pparg*$^{fl/fl}$ *Villin*$^{cre/-}$) or littermate controls (*Pparg*$^{fl/fl}$ *Villin*$^{-/-}$).

(A) *Nos2* transcript levels were determined by quantitative real-time PCR in RNA isolated from preparations of the colonic epithelium.

(B) Nitrate concentrations in mucus scrapings were determined by a modified Griess assay.

(A and B) The boxes in the whisker blot represent the first to third quartiles, and the line indicates the median value. Each dot represents data from one animal.

(C and D) Groups of mice lacking expression of *Pparg* in the intestinal epithelium (*Pparg*$^{fl/fl}$ *Villin*$^{cre/-}$) or littermate controls (*Pparg*$^{fl/fl}$ *Villin*$^{-/-}$) were infected with the indicated *S.* Typhimurium (STm) or *E. coli* (EcN) strain mixtures.

(C) The competitive index in colon contents was determined 4 days after infection. Each dot represents data from one animal. Bars represent geometric mean ± geometric error.

(D) Histological sections of the cecum were blinded and scored for lesions by a veterinary pathologist. Each bar represents data from one animal. *$p < 0.05$; **$p < 0.01$; ns, $p > 0.05$.

E. coli in a closer interquartile range of distance from the actin brush border compared with avirulent *S.* Typhimurium requires motility and chemotaxis (Figure 1H), we reasoned that the difference between the species could be explained either (1) by additional chemotaxis receptors in *E. coli* that mediate attraction to the mucosal surface or (2) by additional chemotaxis receptors in *S.* Typhimurium that mediate repulsion from the mucosal surface. The first possibility was inconsistent with the fact that all three chemotaxis receptors encoded in the *E. coli* Nissle 1917 genome (Tsr, Tar, and Aer) are also present in *S.* Typhimurium (Figure 5A). *E. coli* Nissle 1917 lacks Trg, a chemotaxis receptor present in other commensal *E. coli* strains and *S.* Typhimurium. Notably, *S.* Typhimurium encodes three chemotaxis receptors, McpA, McpB, and McpC, that are not present in *E. coli* (Frye et al., 2006). Two of these, McpB and McpC, have previously been shown to cooperate in mediating a repellent response to avoid oxidative conditions (Lazova et al., 2012). We thus postulated that McpB and McpC repel *S.* Typhimurium from oxidative conditions at the mucosal surface to limit its access to epithelial-derived nitrate. This hypothesis predicted that genetic ablation of McpB and McpC would enable avirulent *S.* Typhimurium (*invA spiB* mutant) to respire nitrate. Furthermore, our hypothesis predicted that an *invA spiB mcpB mcpC* mutant would perform nitrate respiration using NarG, a genetic marker for nitrate respiration in the nutrient niche occupied by *E. coli* (Figure 2A). Consistent with previous results (Figure 2B), *narG* did not confer a fitness advantage when streptomycin-pretreated mice were infected with a 1:1 mixture of an avirulent *S.* Typhimurium strain (*invA spiB* mutant) and an isogenic *narG* mutant (Figure 5B). In support of our hypothesis, mutations in *mcpB* and *mcpC* provided avirulent *S.* Typhimurium with a *narG*-dependent growth benefit, as indicated by increased recovery of an *invA spiB mcpB mcpC* mutant over an *invA spiB mcpB mcpC narG* mutant.

To determine whether a *S.* Typhimurium *invA spiB mcpB mcpC* mutant localizes to a similar spatial niche as commensal *E. coli* Nissle 1917, we used immunofluorescence microscopy to determine the distribution of bacteria within the intestinal lumen by segmenting images and measuring distances from representative bacterial seed pixels to the actin brush border of the epithelium (Figures 1E and 1F). We found that compared with a *S.* Typhimurium *invA spiB* mutant, a *S.* Typhimurium *invA spiB mcpB mcpC* mutant was concentrated significantly closer to the brush border (Figure 5C), suggesting that the deletion of *mcpB* and *mpcC* changes bacterial localization in the gut lumen.

These data suggest that differences in the chemotaxis receptor repertoire between commensal *E. coli* and avirulent *S.* Typhimurium help explain why only the former can access a nutrient niche containing epithelial-derived nitrate.

E. coli uses nitrate respiration to confer niche protection against *Salmonella*

Finally, we wanted to determine whether invasion of the nutrient niche constructed by *S.* Typhimurium virulence factors (Figure 3G) enables commensal *E. coli* to compete with the pathogen for nitrate. To this end, streptomycin-treated mice were inoculated with *E. coli* strains that were either proficient for motility and nitrate respiration (*E. coli* Nissle 1917 wild type), nonmotile (*fliC* mutant), or deficient for nitrate respiration (*narZ narG napA* mutant). 2 days later, mice were challenged with a 1:1 mixture of the virulent *S.* Typhimurium wild type and a nitrate-respiration-deficient strain (*S.* Typhimurium *narZ narG napA* mutant) to assess the pathogen's ability to colonize the intestine and respire nitrate. Colonization with *E. coli* prior to *S.* Typhimurium challenge markedly reduced numbers of the pathogen in cecal contents (Figure 6A), which was consistent with previous reports showing that commensal *E. coli*

Please cite this article in press as: Liou et al., Host cells subdivide nutrient niches into discrete biogeographical microhabitats for gut microbes, Cell Host & Microbe (2022), https://doi.org/10.1016/j.chom.2022.04.012

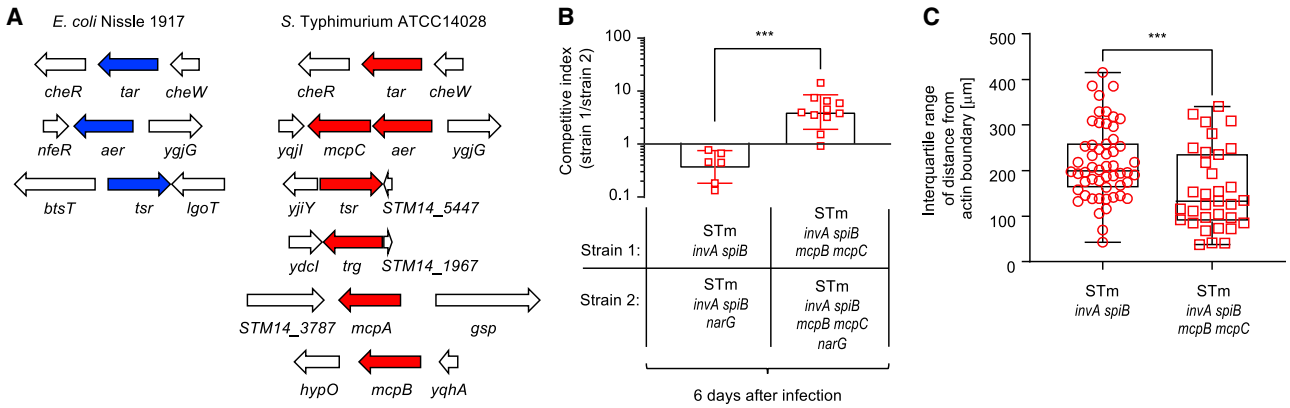

Figure 5. McpB and McpC exclude *S.* Typhimurium from a nutrient-niche-containing nitrate

(A) Genetic repertoire of chemotaxis receptor genes (blue and red arrows) in *E. coli* Nissle 1917 (left panel) and *S.* Typhimurium strain ATCC14028 (right panel).

(B) Groups of streptomycin-pretreated C57BL/6J mice were infected with the indicated mixtures of avirulent *S.* Typhimurium (STm) strains, and cecal contents were collected 6 days after infection to determine the competitive index. Bars represent geometric mean ± geometric error.

(C) Groups (N = 8) of streptomycin-treated mice were infected with one of the indicated *S.* Typhimurium strains, and the cecum was collected for sectioning 2 days later. The boxes in the whisker blot represent the first to third quartiles, and the line indicates the median value of the interquartile range of distances from the actin boundary. Each symbol (dots/squares) represents data from one microscopic image. ***$p < 0.001$.

contribute to colonization resistance against *S.* Typhimurium (Eberl et al., 2021; Velazquez et al., 2019; Wotzka et al., 2019). Notably, *E. coli* strains that were either nitrate-respiration deficient (*E. coli narZ narG napA* mutant) or nonmotile (*E. coli fliC* mutant) were less potent in reducing numbers of *S.* Typhimurium during a challenge (Figure 6A). Nitrate respiration provided a fitness advantage to *S.* Typhimurium in streptomycin-pretreated mice, as indicated by the recovery of higher numbers of the *S.* Typhimurium wild type compared with a nitrate-respiration-deficient (*narZ narG napA*) mutant (Figure 6B). However, colonization with wild-type *E. coli* prior to *S.* Typhimurium challenge abrogated the fitness advantage conferred by nitrate respiration, as indicated by recovery of equal numbers of the *S.* Typhimurium wild type and a *narZ narG napA* mutant. Notably, the fitness advantage conferred by nitrate respiration in *S.* Typhimurium was restored when mice were colonized with a nitrate-respiration-deficient *E. coli* strain (*narZ narG napA* mutant) prior to *S.* Typhimurium challenge, suggesting that *E. coli* competes with *S.* Typhimurium for nitrate. Furthermore, *E. coli* required motility to compete with *S.* Typhimurium for nitrate, because nitrate respiration provided a fitness advantage for *S.* Typhimurium when mice were colonized with a nonmotile *E. coli* strain (*fliC* mutant) prior to pathogen challenge. Collectively, these results supported the idea that commensal *E. coli* use motility and nitrate respiration to compete with *S.* Typhimurium for resources critical for pathogen expansion in the intestinal lumen.

To further assess competition between commensal *E. coli* and avirulent *S.* Typhimurium, streptomycin-treated mice were inoculated with both species simultaneously. Avirulent *S.* Typhimurium (*invA spiB* mutant) colonized the murine cecum at higher levels than *E. coli* Nissle 1917, which was at least in part due to McpB/McpC-mediated chemotaxis, because the fitness advantage over *E. coli* was markedly reduced for a *S.* Typhimurium *invA spiB mcpB mcpC* mutant (Figure 6C).

DISCUSSION

Changes in the microbiota composition are associated with numerous human diseases, thus making an analysis of the factors that govern strain engraftment and abundance relevant for understanding the underlying disease process. Conventional wisdom holds that each nutrient niche in the gut ecosystem is defined by critical resources, the abundance of which determines the abundance of its microbial occupant (Freter et al., 1983). However, here we show that a nutrient niche defined by a critical resource can be further subdivided by the host biogeographically into distinct microhabitats (Figure 6D), a process predicted to increase the number of nutrient niches that are present, which in turn will increase the number of similar coexisting species.

The idea that critical resources determine taxa abundance is supported by work on primary fermenters of dietary fibers or glycans. Dietary fiber escapes digestion by host enzymes in the upper gastrointestinal tract and serves as a critical resource for fiber-consuming bacteria (“fiber eaters”) in the colon. A prolonged reduction in dietary fiber intake leads to an irreversible extinction of fiber eaters that rely solely on this critical resource, whereas fiber eaters that can switch to consuming other critical resources, such as host-derived mucin glycans, can persist in the gut microbiota during periods of dietary fiber starvation (Desai et al., 2016; Sonnenburg et al., 2016; Sonnenburg et al., 2005). Conversely, dietary supplementation with a complex polysaccharide that is not utilized by any member of the microbiota generates a new nutrient niche that supports engraftment of a fiber-eater that harbors genes necessary to catabolize it (Shepherd et al., 2018). As a result, the presence or absence of critical resources can drive changes in the microbiota composition.

Host-derived respiratory electron acceptors, such as oxygen and nitrate, are critical resources whose abundance determines the abundance of facultative anaerobic bacteria, such as

Please cite this article in press as: Liou et al., Host cells subdivide nutrient niches into discrete biogeographical microhabitats for gut microbes, Cell Host & Microbe (2022), https://doi.org/10.1016/j.chom.2022.04.012

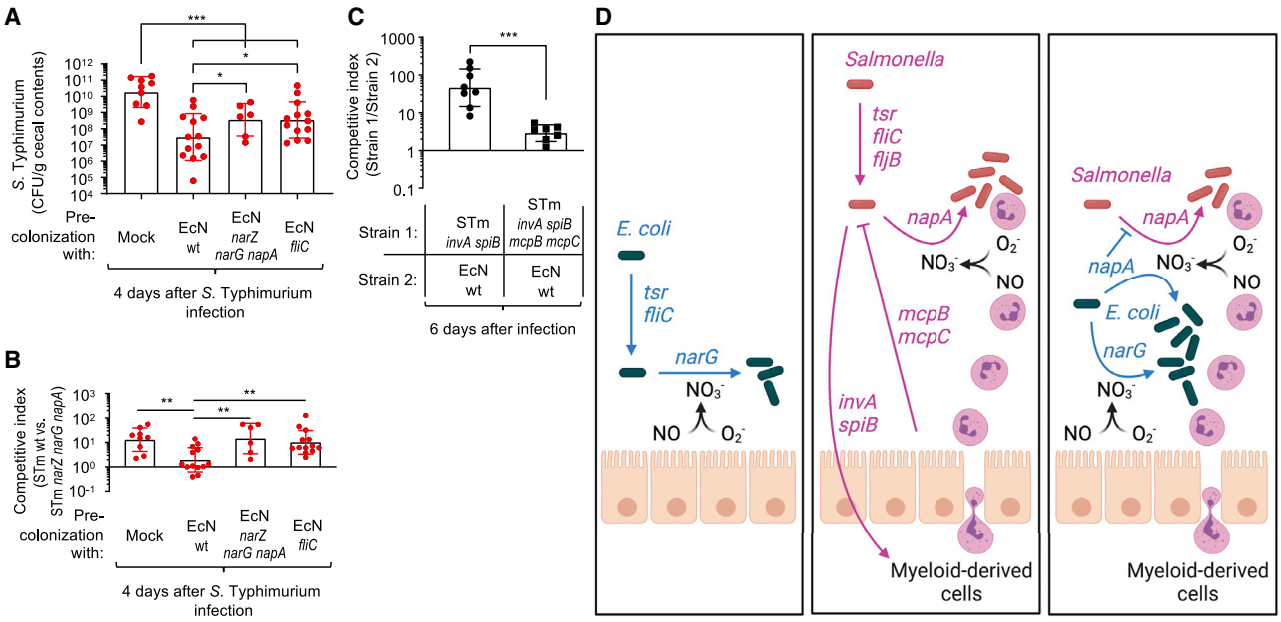

Figure 6. *E. coli* uses nitrate respiration to confer colonization resistance against *Salmonella*

(A and B) Groups of streptomycin-pretreated C57BL/6J mice were inoculated with sterile LB broth (Mock) or with the indicated *E. coli* Nissle 1917 (EcN) strains. Two days after inoculation with *E. coli*, mice were challenged with a 1:1 mixture of *S.* Typhimurium (STm) wild type (WT) and a nitrate-respiration-deficient mutant (*narZ narG napA*).

(A) Total numbers of *S.* Typhimurium recovered from cecal contents.

(B) Competitive index of the indicated *S.* Typhimurium strains.

(C) Groups of streptomycin-pretreated C57BL/6J mice were inoculated with the indicated mixtures of *S.* Typhimurium and *E. coli* strains. The graph shows the competitive index comparing fitness of the *S.* Typhimurium strain with the *E. coli* strain. Bars represent geometric mean ± geometric error. Each symbol (circles or squares) represents data from one animal. *$p < 0.05$; **$p < 0.01$; ***$p < 0.001$.

(D) Model for the nutrient niche occupied by commensal *E. coli* (left panel), virulent *S.* Typhimurium (middle panel) and the competition between both species for nitrate (right panel). Created with BioRender.com. NO, nitric oxide; O_2^-, superoxide radical; NO_3^-, nitrate.

members of the *Enterobacterales*, within the colonic microbiota (reviewed in the studies conducted by Rogers et al., 2021 and Winter et al., 2013a). During homeostasis, *Enterobacterales* likely maintain themselves using the limited amount of oxygen emanating from the mucosal surface. Surprisingly, the bioavailability of oxygen in the large intestine is not limited to a niche in close proximity to the mucosal surface, because the growth benefit conferred by aerobic respiration is not enhanced when bacteria are attached to the epithelial surface compared with bacteria occupying a niche in the intestinal lumen (Miller et al., 2020). During homeostasis, the host produces nitrate constitutively in the ileum (Rivera-Chávez et al., 2016a), but this electron acceptor is not available in the colon. The low abundance of respiratory electron acceptors in the large intestine during homeostasis relegates *Enterobacterales* to an existence as minority species (Byndloss et al., 2017). However, conditions of intestinal inflammation or environmental exposure to antibiotics or Western-style high-fat diet increases the availability of respiratory electron acceptors in the colon, thereby driving dysbiosis characterized by an expansion of commensal *Enterobacterales* in the fecal microbiota (Byndloss et al., 2017; Cevallos et al., 2019; Chanin et al., 2020; Hughes et al., 2017; Lee et al., 2020; Pötgens et al., 2018; Spees et al., 2013; Wang et al., 2019; Winter et al., 2013b; Yoo et al., 2021; Zhu et al., 2019, 2018). Treatment of mice with streptomycin induces *Nos2* expression in the colonic epithelium, which increases luminal nitrate levels to enhance growth of *E. coli* by nitrate respiration (Byndloss et al., 2017; Jones et al., 2011; Spees et al., 2013). We used streptomycin-treated mice to study nutrient niches containing host-derived nitrate, but a limitation of this approach is that an antibiotic-mediated disruption of the gut microbiota depletes short-chain fatty acids (Meynell, 1963; Meynell and Subbaiah, 1963). Therefore, we also validated our results in a mouse model with genetically elevated *Nos2* expression in the colonic epithelium (*Pparg*$^{fl/fl}$*Villin*$^{cre/-}$ mice), in which the microbiota remains undisturbed and produces normal levels of short-chain fatty acids (Byndloss et al., 2017).

Here we show that niche opportunities for *Enterobacterales* are not solely created by an increased abundance of critical resources; their formation also involves the construction of distinct microhabitats in which these resources become available. For example, antibiotic treatment increases the availability of nitrate in the colon (Byndloss et al., 2017; Spees et al., 2013). Similarly, *S.* Typhimurium-induced inflammation constructs a nutrient niche in which nitrate fuels pathogen growth (Lopez et al., 2015, 2012; McLaughlin et al., 2019; Rivera-Chávez et al., 2016b). *S.* Typhimurium-induced inflammation increased the availability of phagocyte-derived nitrate, a resource utilized by commensal *E. coli* during coinfection. Commensal *E. coli* was able to invade the nutrient niche constructed by virulence factors

of the pathogen and compete with *S.* Typhimurium for nitrate, which contributed to its ability to confer colonization resistance. The finding that competition for nitrate only partially accounted for protection conferred by *E. coli* against *S.* Typhimurium challenge is consistent with the finding that additional factors contribute to colonization resistance, including microcin production by *E. coli* (Sassone-Corsi et al., 2016), and competition for other critical resources, such as oxygen (Velazquez et al., 2019) and polyols (Eberl et al., 2021).

Notably, the nutrient niche constructed by antibiotic treatment provided access to epithelial-derived nitrate, which could be exploited only by a commensal *E. coli* strain, and not by an avirulent *S.* Typhimurium strain. The underlying mechanism was the presence of two chemotaxis receptors in *S.* Typhimurium, termed McpB and McpC, which cooperate to repel the pathogen from oxidative conditions (Lazova et al., 2012). Interestingly, a commensal *E. coli* strain occupied an ecological position in closer proximity to the mucosal surface compared with an avirulent *S.* Typhimurium strain, providing further support for the idea that both organisms occupied distinct nitrate-containing microhabitats. Based on the observation that two *E. coli* strains, which differ in their ability to form biofilms in the mucus layer, can co-colonize the streptomycin-treated mouse gut (Leatham-Jensen et al., 2012), the "restaurant hypothesis" proposes that microbes consuming the same critical resources can co-exist if they occupy spatially distinct niches (Pereira and Berry, 2017). However, the role the host plays in providing different spatial niches has remained unexplored. Our data support the concept that different host-cell types can create distinct spatial microhabitats containing the same critical resource, host-derived nitrate, thereby providing niche opportunities for distinct bacterial species (Figure 6D). Thus, by shaping the biogeographical diversity of the gut microbiota, the host can enlarge the number of available ecological positions, which is predicted to increase the number of coexisting species within the gut microbiota. The spatial microhabitats generated by the host are lost in the test tube, which likely contributes to the reduction in diversity of host-associated microbial communities observed upon *in vitro* culture (Ahmadi et al., 2019; Kim et al., 2011).

STAR★METHODS

Detailed methods are provided in the online version of this paper and include the following:

- KEY RESOURCES TABLE
- RESOURCE AVAILABILITY
  - Lead contact
  - Materials availability
  - Data and code availability
- EXPERIMENTAL MODEL AND SUBJECT DETAILS
  - Animal experiments
  - Bacterial strains and culture conditions
- METHOD DETAILS
  - Construction of *E. coli* mutants
  - Construction of *S. Typhimurium* mutants
  - Phage transduction
  - Nitrate measurements
  - Generation of bone marrow chimeras
  - Flow cytometry and tissue processing
  - RNA isolation and quantitative real-time PCR
  - Histopathology
  - Detection of myeloperoxidase
  - Fluorescence imaging
  - Segmentation of immunofluorescence images
- QUANTIFICATION AND STATISTICAL ANALYSIS
  - Quantification of bacterial distance from epithelium
  - Statistical analysis

SUPPLEMENTAL INFORMATION

Supplemental information can be found online at https://doi.org/10.1016/j.chom.2022.04.012.

ACKNOWLEDGMENTS

Y.L. was supported by a Vaadia-BARD Postdoctoral Fellowship FI-505-2014 and United States-Israel Binational Science Foundation grant 2019136. H.H. was supported by a UC Davis Academic Federation Innovative Development Award, a research grant from Takeda Science Foundation, a fellowship from the Daiichi Sankyo Foundation of Life Science, and JSPS KAKENHI grant number JP21K07027. Work in M.X.B.'s laboratory was supported by grant V2020-013 from the V Foundation for Cancer Research and United States-Israel Binational Science Foundation grant 2019136. Work in A.J.B.'s lab was supported by Crohn's and Colitis Foundation of America Senior Investigator Award # 650976. Public Health Service grants provided support for H.H. (AI143929), S.I.S. (AI129302), D.E.N. (HL152621), J.A.R. (AI060555), M.X.B. (DK131104), R.M.H. (GM118085 and AI158295), S.R.C. (DP2HD094656), S.J.M. (AI139410 and AI139047), and A.J.B. (AI044170, AI096528, AI112445, AI112949, and AI153069). The project described was supported by the National Center for Advancing Translational Sciences, National Institutes of Health, through grant number UL1 TR000002 and linked award TL1 TR000133 (H.P.S.). The content is solely the responsibility of the authors and does not necessarily represent the official views of the NIH.

AUTHOR CONTRIBUTIONS

Conceptualization, M.J.L., B.M.M., H.H., S.R.C., S.J.M., M.X.B., S.I.S., and A.J.B.; methodology, M.J.L., B.M.M., Y.L., H.N., D.E.N., H.P.S., J.A.R., S.P.M., H.H., A.W.L.R., E.M.V., B.P.B., S.R.C., S.J.M., R.M.H., M.X.B., S.I.S., and A.J.B.; investigation, M.J.L., B.M.M, Y.L., H.N., D.E.N., H.P.S., J.A.R., S.P.M., H.H., A.W.L.R., E.M.V., and B.P.B.; resources, S.R.C., S.J.M., R.M.H., and A.J.B.; funding acquisition, H.P.S., H.H., Y.L., and A.J.B.; writing—original draft, M.J.L. and A.J.B.; writing—review and editing, M.J.L. and A.J.B.; supervision, Y.L., H.H., S.R.C., S.J.M., M.X.B., S.I.S., and A.J.B.

DECLARATION OF INTERESTS

The authors declare no competing interests.

Received: April 16, 2021
Revised: March 15, 2022
Accepted: April 20, 2022
Published: May 13, 2022

REFERENCES

Adeolu, M., Alnajar, S., Naushad, S., and Gupta, R.S. (2016). Genome-based phylogeny and taxonomy of the 'Enterobacteriales': proposal for *Enterobacterales* ord. nov. divided into the families *Enterobacteriaceae*, *Erwiniaceae* fam. nov., *Pectobacteriaceae* fam. nov., *Yersiniaceae* fam. nov., *Hafniaceae* fam. nov., *Morganellaceae* fam. nov., and *Budviciaceae* fam. nov. Int. J. Syst. Evol. Microbiol. *66*, 5575–5599.

Ahmadi, S., Wang, S., Nagpal, R., Mainali, R., Soleimanian-Zad, S., Kitzman, D., and Yadav, H. (2019). An in vitro batch-culture model to estimate the effects of interventional regimens on human fecal microbiota. J. Vis. Exp. e59524.

Barthel, M., Hapfelmeier, S., Quintanilla-Martínez, L., Kremer, M., Rohde, M., Hogardt, M., Pfeffer, K., Rüssmann, H., and Hardt, W.D. (2003). Pretreatment of mice with streptomycin provides a *Salmonella enterica* serovar Typhimurium colitis model that allows analysis of both pathogen and host. Infect. Immun. *71*, 2839–2858.

Byndloss, M.X., Olsan, E.E., Rivera-Chávez, F., Tiffany, C.R., Cevallos, S.A., Lokken, K.L., Torres, T.P., Byndloss, A.J., Faber, F., Gao, Y., et al. (2017). Microbiota-activated PPAR- γ signaling inhibits dysbiotic Enterobacteriaceae expansion. Science *357*, 570–575.

Cevallos, S.A., Lee, J.Y., Tiffany, C.R., Byndloss, A.J., Johnston, L., Byndloss, M.X., and Bäumler, A.J. (2019). Increased epithelial oxygenation links colitis to an expansion of tumorigenic bacteria. mBio *10*, e02244-19.

Chanin, R.B., Winter, M.G., Spiga, L., Hughes, E.R., Zhu, W., Taylor, S.J., Arenales, A., Gillis, C.C., Büttner, L., Jimenez, A.G., et al. (2020). Epithelial-derived reactive oxygen species enable AppBCX-mediated aerobic respiration of *Escherichia coli* during intestinal inflammation. Cell Host Microbe *28*, 780–788.e5.

David, L.A., Materna, A.C., Friedman, J., Campos-Baptista, M.I., Blackburn, M.C., Perrotta, A., Erdman, S.E., and Alm, E.J. (2014). Host lifestyle affects human microbiota on daily timescales. Genome Biol. *15*, R89.

Desai, M.S., Seekatz, A.M., Koropatkin, N.M., Kamada, N., Hickey, C.A., Wolter, M., Pudlo, N.A., Kitamoto, S., Terrapon, N., Muller, A., et al. (2016). A dietary fiber-deprived gut microbiota degrades the colonic mucus barrier and enhances pathogen susceptibility. Cell *167*, 1339–1353.e21.

Eberl, C., Weiss, A.S., Jochum, L.M., Durai Raj, A.C., Ring, D., Hussain, S., Herp, S., Meng, C., Kleigrewe, K., Gigl, M., et al. (2021). *E. coli* enhance colonization resistance against *Salmonella* Typhimurium by competing for galactitol, a context-dependent limiting carbon source. Cell Host Microbe *29*, 1680–1692.e7.

El Kaoutari, A., Armougom, F., Gordon, J.I., Raoult, D., and Henrissat, B. (2013). The abundance and variety of carbohydrate-active enzymes in the human gut microbiota. Nat. Rev. Microbiol. *11*, 497–504.

Faust, N., Varas, F., Kelly, L.M., Heck, S., and Graf, T. (2000). Insertion of enhanced green fluorescent protein into the lysozyme gene creates mice with green fluorescent granulocytes and macrophages. Blood *96*, 719–726.

Freter, R., Brickner, H., Fekete, J., Vickerman, M.M., and Carey, K.E. (1983). Survival and implantation of *Escherichia coli* in the intestinal tract. Infect. Immun. *39*, 686–703.

Frye, J., Karlinsey, J.E., Felise, H.R., Marzolf, B., Dowidar, N., McClelland, M., and Hughes, K.T. (2006). Identification of new flagellar genes of *Salmonella enterica* serovar Typhimurium. J. Bacteriol. *188*, 2233–2243.

Gillis, C.C., Hughes, E.R., Spiga, L., Winter, M.G., Zhu, W., Furtado de Carvalho, T., Chanin, R.B., Behrendt, C.L., Hooper, L.V., Santos, R.L., and Winter, S.E. (2018). Dysbiosis-associated change in host metabolism generates lactate to support *Salmonella* growth. Cell Host Microbe *23*, 54–64.e6.

Greer-Phillips, S.E., Alexandre, G., Taylor, B.L., and Zhulin, I.B. (2003). Aer and Tsr guide *Escherichia coli* in spatial gradients of oxidizable substrates. Microbiology (Reading) *149*, 2661–2667.

Hapfelmeier, S., Stecher, B., Barthel, M., Kremer, M., Müller, A.J., Heikenwalder, M., Stallmach, T., Hensel, M., Pfeffer, K., Akira, S., and Hardt, W.-D. (2005). The Salmonella pathogenicity island (SPI)-2 and SPI-1 type III secretion systems allow *Salmonella* serovar *typhimurium* to trigger colitis via MyD88-dependent and MyD88-independent mechanisms. J. Immunol. *174*, 1675–1685.

Hughes, E.R., Winter, M.G., Duerkop, B.A., Spiga, L., Furtado de Carvalho, T., Zhu, W., Gillis, C.C., Büttner, L., Smoot, M.P., Behrendt, C.L., et al. (2017). Microbial respiration and formate oxidation as metabolic signatures of inflammation-associated dysbiosis. Cell Host Microbe *21*, 208–219.

Human Microbiome Project Consortium. (2012). Structure, function and diversity of the healthy human microbiome. Nature *486*, 207–214.

Jones, S.A., Chowdhury, F.Z., Fabich, A.J., Anderson, A., Schreiner, D.M., House, A.L., Autieri, S.M., Leatham, M.P., Lins, J.J., Jorgensen, M., et al. (2007). Respiration of *Escherichia coli* in the mouse intestine. Infect. Immun. *75*, 4891–4899.

Jones, S.A., Gibson, T., Maltby, R.C., Chowdhury, F.Z., Stewart, V., Cohen, P.S., and Conway, T. (2011). Anaerobic respiration of Escherichia coli in the mouse intestine. Infect. Immun. *79*, 4218–4226.

Kim, B.-S., Kim, J.N., and Cerniglia, C.E. (2011). *In vitro* culture conditions for maintaining a complex population of human gastrointestinal tract microbiota. J. Biomed. Biotechnol. *2011*, 838040.

Lazova, M.D., Butler, M.T., Shimizu, T.S., and Harshey, R.M. (2012). *Salmonella* chemoreceptors McpB and McpC mediate a repellent response to *L*-cystine: a potential mechanism to avoid oxidative conditions. Mol. Microbiol. *84*, 697–711.

Leatham-Jensen, M.P., Frimodt-Møller, J., Adediran, J., Mokszycki, M.E., Banner, M.E., Caughron, J.E., Krogfelt, K.A., Conway, T., and Cohen, P.S. (2012). The streptomycin-treated mouse intestine selects *Escherichia coli* envZ missense mutants that interact with dense and diverse intestinal microbiota. Infect. Immun. *80*, 1716–1727.

Lee, J.Y., Cevallos, S.A., Byndloss, M.X., Tiffany, C.R., Olsan, E.E., Butler, B.P., Young, B.M., Rogers, A.W.L., Nguyen, H., Kim, K., et al. (2020). High-fat diet and antibiotics cooperatively impair mitochondrial bioenergetics to trigger dysbiosis that exacerbates pre-inflammatory bowel disease. Cell Host Microbe *28*, 273–284.e6.

Ley, R.E., Hamady, M., Lozupone, C., Turnbaugh, P.J., Ramey, R.R., Bircher, J.S., Schlegel, M.L., Tucker, T.A., Schrenzel, M.D., Knight, R., and Gordon, J.I. (2008). Evolution of mammals and their gut microbes. Science *320*, 1647–1651.

Loetscher, Y., Wieser, A., Lengefeld, J., Kaiser, P., Schubert, S., Heikenwalder, M., Hardt, W.D., and Stecher, B. (2012). Salmonella transiently reside in luminal neutrophils in the inflamed gut. PLoS One *7*, e34812.

Lopez, C.A., Rivera-Chávez, F., Byndloss, M.X., and Bäumler, A.J. (2015). The periplasmic nitrate reductase NapABC supports luminal growth of *Salmonella enterica* serovar Typhimurium during colitis. Infect. Immun. *83*, 3470–3478.

Lopez, C.A., Winter, S.E., Rivera-Chávez, F., Xavier, M.N., Poon, V., Nuccio, S.P., Tsolis, R.M., and Bäumler, A.J. (2012). Phage-mediated acquisition of a type III secreted effector protein boosts growth of *Salmonella* by nitrate respiration. mBio *3*, e00143-12.

Matsuda, S., Haneda, T., Saito, H., Miki, T., and Okada, N. (2019). *Salmonella enterica* effectors SifA, SpvB, SseF, SseJ, and SteA contribute to type III secretion system 1-independent inflammation in a streptomycin-pretreated mouse model of colitis. Infect. Immun. *87*, e00872-18.

McLaughlin, P.A., Bettke, J.A., Tam, J.W., Leeds, J., Bliska, J.B., Butler, B.P., and van der Velden, A.W.M. (2019). Inflammatory monocytes provide a niche for *Salmonella* expansion in the lumen of the inflamed intestine. PLoS Pathog. *15*, e1007847.

Meynell, G.G. (1963). Antibacterial mechanisms of the mouse gut. II. The role of Eh and volatile fatty acids in the normal gut. Br. J. Exp. Pathol. *44*, 209–219.

Meynell, G.G., and Subbaiah, T.V. (1963). Antibacterial mechanisms of the mouse gut. I. Kinetics of infection by Salmonella typhi-murium in normal and streptomycin-treated mice studied with abortive transductants. Br. J. Exp. Pathol. *44*, 197–208.

Miller, B.M., Liou, M.J., Zhang, L.F., Nguyen, H., Litvak, Y., Schorr, E.M., Jang, K.K., Tiffany, C.R., Butler, B.P., and Bäumler, A.J. (2020). Anaerobic respiration of NOX1-derived hydrogen peroxide licenses bacterial growth at the colonic surface. Cell Host Microbe *28*, 789–797.e5.

Nissle, A. (1925). Weiteres über Grundlagen und Praxis der Mutaflorbehandlung. Dtsch. Med. Wochenschr. *51*, 1809–1813.

Pereira, F.C., and Berry, D. (2017). Microbial nutrient niches in the gut. Environ. Microbiol. *19*, 1366–1378.

Pötgens, S.A., Brossel, H., Sboarina, M., Catry, E., Cani, P.D., Neyrinck, A.M., Delzenne, N.M., and Bindels, L.B. (2018). *Klebsiella oxytoca* expands in cancer

cachexia and acts as a gut pathobiont contributing to intestinal dysfunction. Sci. Rep. *8*, 12321.

Qin, J., Li, R., Raes, J., Arumugam, M., Burgdorf, K.S., Manichanh, C., Nielsen, T., Pons, N., Levenez, F., Yamada, T., et al. (2010). A human gut microbial gene catalogue established by metagenomic sequencing. Nature *464*, 59–65.

Rebbapragada, A., Johnson, M.S., Harding, G.P., Zuccarelli, A.J., Fletcher, H.M., Zhulin, I.B., and Taylor, B.L. (1997). The Aer protein and the serine chemoreceptor Tsr independently sense intracellular energy levels and transduce oxygen, redox, and energy signals for *Escherichia coli* behavior. Proc. Natl. Acad. Sci. USA *94*, 10541–10546.

Rivera-Chávez, F., Lopez, C.A., Zhang, L.F., García-Pastor, L., Chávez-Arroyo, A., Lokken, K.L., Tsolis, R.M., Winter, S.E., and Bäumler, A.J. (2016a). Energy taxis toward host-derived nitrate supports a *Salmonella* pathogenicity island 1-independent mechanism of invasion. mBio *7*, e00960-16.

Rivera-Chávez, F., Winter, S.E., Lopez, C.A., Xavier, M.N., Winter, M.G., Nuccio, S.P., Russell, J.M., Laughlin, R.C., Lawhon, S.D., Sterzenbach, T., et al. (2013). Salmonella uses energy taxis to benefit from intestinal inflammation. PLoS Pathog. *9*, e1003267.

Rivera-Chávez, F., Zhang, L.F., Faber, F., Lopez, C.A., Byndloss, M.X., Olsan, E.E., Xu, G., Velazquez, E.M., Lebrilla, C.B., Winter, S.E., and Bäumler, A.J. (2016b). Depletion of butyrate-producing *Clostridia* from the gut microbiota drives an aerobic luminal expansion of *Salmonella*. Cell Host Microbe *19*, 443–454.

Rogers, A.W.L., Tsolis, R.M., and Bäumler, A.J. (2021). Salmonella versus the microbiome. Microbiol. Mol. Biol. Rev. *85*.

Rothaeusler, K., and Baumgarth, N. (2006). Evaluation of intranuclear BrdU detection procedures for use in multicolor flow cytometry. Cytometry A *69*, 249–259.

Sassone-Corsi, M., Nuccio, S.P., Liu, H., Hernandez, D., Vu, C.T., Takahashi, A.A., Edwards, R.A., and Raffatellu, M. (2016). Microcins mediate competition among Enterobacteriaceae in the inflamed gut. Nature *540*, 280–283.

Shepherd, E.S., DeLoache, W.C., Pruss, K.M., Whitaker, W.R., and Sonnenburg, J.L. (2018). An exclusive metabolic niche enables strain engraftment in the gut microbiota. Nature *557*, 434–438.

Sonnenburg, E.D., Smits, S.A., Tikhonov, M., Higginbottom, S.K., Wingreen, N.S., and Sonnenburg, J.L. (2016). Diet-induced extinctions in the gut microbiota compound over generations. Nature *529*, 212–215.

Sonnenburg, J.L., Xu, J., Leip, D.D., Chen, C.H., Westover, B.P., Weatherford, J., Buhler, J.D., and Gordon, J.I. (2005). Glycan foraging in vivo by an intestine-adapted bacterial symbiont. Science *307*, 1955–1959.

Spees, A.M., Wangdi, T., Lopez, C.A., Kingsbury, D.D., Xavier, M.N., Winter, S.E., Tsolis, R.M., and Bäumler, A.J. (2013). Streptomycin-induced inflammation enhances *Escherichia coli* gut colonization through nitrate respiration. mBio *4*, e00430-13.

Tsolis, R.M., Adams, L.G., Ficht, T.A., and Bäumler, A.J. (1999). Contribution of *Salmonella typhimurium* virulence factors to diarrheal disease in calves. Infect. Immun. *67*, 4879–4885.

Velazquez, E.M., Nguyen, H., Heasley, K.T., Saechao, C.H., Gil, L.M., Rogers, A.W.L., Miller, B.M., Rolston, M.R., Lopez, C.A., Litvak, Y., et al. (2019). Endogenous Enterobacteriaceae underlie variation in susceptibility to *Salmonella* infection. Nat. Microbiol. *4*, 1057–1064.

Wang, S., El-Fahmawi, A., Christian, D.A., Fang, Q., Radaelli, E., Chen, L., Sullivan, M.C., Misic, A.M., Ellringer, J.A., Zhu, X.Q., et al. (2019). Infection-induced intestinal dysbiosis is mediated by macrophage activation and nitrate production. mBio *10*, e00935-19.

Winter, S.E., Lopez, C.A., and Bäumler, A.J. (2013a). The dynamics of gut-associated microbial communities during inflammation. EMBO Rep. *14*, 319–327.

Winter, S.E., Thiennimitr, P., Winter, M.G., Butler, B.P., Huseby, D.L., Crawford, R.W., Russell, J.M., Bevins, C.L., Adams, L.G., Tsolis, R.M., et al. (2010). Gut inflammation provides a respiratory electron acceptor for *Salmonella*. Nature *467*, 426–429.

Winter, S.E., Winter, M.G., Xavier, M.N., Thiennimitr, P., Poon, V., Keestra, A.M., Laughlin, R.C., Gomez, G., Wu, J., Lawhon, S.D., et al. (2013b). Host-derived nitrate boosts growth of *E. coli* in the inflamed gut. Science *339*, 708–711.

Wotzka, S.Y., Kreuzer, M., Maier, L., Arnoldini, M., Nguyen, B.D., Brachmann, A.O., Berthold, D.L., Zünd, M., Hausmann, A., Bakkeren, E., et al. (2019). *Escherichia coli* limits *Salmonella* Typhimurium infections after diet shifts and fat-mediated microbiota perturbation in mice. Nat. Microbiol. *4*, 2164–2174.

Yoo, W., Zieba, J.K., Foegeding, N.J., Torres, T.P., Shelton, C.D., Shealy, N.G., Byndloss, A.J., Cevallos, S.A., Gertz, E., Tiffany, C.R., et al. (2021). High-fat diet-induced colonocyte dysfunction escalates microbiota-derived trimethylamine *N*-oxide. Science *373*, 813–818.

Zhang, S., Santos, R.L., Tsolis, R.M., Stender, S., Hardt, W.D., Bäumler, A.J., and Adams, L.G. (2002). The *Salmonella enterica* serotype typhimurium effector proteins SipA, SopA, SopB, SopD, and SopE2 act in concert to induce diarrhea in calves. Infect. Immun. *70*, 3843–3855.

Zhu, W., Miyata, N., Winter, M.G., Arenales, A., Hughes, E.R., Spiga, L., Kim, J., Sifuentes-Dominguez, L., Starokadomskyy, P., Gopal, P., et al. (2019). Editing of the gut microbiota reduces carcinogenesis in mouse models of colitis-associated colorectal cancer. J. Exp. Med. *216*, 2378–2393.

Zhu, W., Winter, M.G., Byndloss, M.X., Spiga, L., Duerkop, B.A., Hughes, E.R., Büttner, L., de Lima Romão, E., Behrendt, C.L., Lopez, C.A., et al. (2018). Precision editing of the gut microbiota ameliorates colitis. Nature *553*, 208–211.

Please cite this article in press as: Liou et al., Host cells subdivide nutrient niches into discrete biogeographical microhabitats for gut microbes, Cell Host & Microbe (2022), https://doi.org/10.1016/j.chom.2022.04.012

STAR★METHODS

KEY RESOURCES TABLE

REAGENT or RESOURCE	SOURCE	IDENTIFIER
Antibodies		
*InVivo*MAb anti-mouse Ly-6G (1A8)	Bio X Cell	Cat#BE0075-1
*InVivo*MAb rat IgG2a isotype control, anti-trinitrophenol (2A3)	Bio X Cell	Cat# BE0089
*InVivo*MAb rat IgG2b isotype control, anti-keyhole limpet hemocyanin (LTF-2)	Bio X Cell	Cat# BE0090
Salmonella O Antiserum Factor 12	Becton Dickinson	Cat# 227791
Goat IgG Fraction to Mouse Complement C3	MP Biomedicals	ICN 55463
Alexa Fluor 568 donkey anti-rabbit IgG (H+L)	Invitrogen	Cat # A10042
Alexa Fluor 568 donkey anti-goat IgG (H+L)	Invitrogen	Cat # A11057
Alexa Fluor 488 donkey anti-mouse IgG (H+L)	Invitrogen	Cat # A21202
PE anti-mouse CD3 (17A2)	BioLegend	Cat # 100206
PE anti-mouse/human CD45R/B220 (RA3-6B2)	BioLegend	Cat # 103207
PE anti-mouse NK-1.1 (PK136)	BioLegend	Cat # 108708
PE/Cy7 anti-mouse/human CD11b (M1/70)	BioLegend	Cat # 101215
Brilliant Violet 421 anti-mouse CD115 (CSF-1R) (AFS98)	BioLegend	Cat # 135513
APC Ly-6G/Ly-6C Monoclonal Antibody (RB6-8C5)	eBioscience	Cat# 17-5931-82
Bacterial and virus strains		
For strains used in this study see Table S1	see Table S1	see Table S1
Biological samples		
For plasmids used in this study see Table S1	see Table S1	see Table S1
Chemicals, peptides, and recombinant proteins		
Digitonin	Sigma-Aldrich	Product # D141
Saponin	Sigma-Aldrich	Product # S4521
Diphenyleneiodonium chloride (DPI)	Sigma-Aldrich	Product # D2926
Chloroquine diphosphate salt	Sigma-Aldrich	Product # C6628
Hoechst 33342	Invitrogen	Cat # H3570
ProLong™ Diamond Antifade Mountant	Invitrogen	Cat # P36965
Hydrogen peroxide	EMD	Cat # HX0635
Luminol	Sigma-Aldrich	Product # 123072
BD Cytofix™ Fixation buffer	Becton Dickinson	Cat # 554655
Live/Dead Fixable Aqua Dead Cell Stain kit	Invitrogen	Cat # L34957
Critical commercial assays		
TRI-reagent	Molecular Research Center	Cat # TR118
DNA-free DNA Removal Kit	Applied Biosystems	Cat# AM1906
SYBR Green PCR Master Mix	Applied Biosystems	Cat # 4309155
Zymoclean Gel DNA Recovery Kit	Zymo Research	Cat# D4001
QIAprep Spin Miniprep Kit	Qiagen	Cat# 27106
Experimental models: Organisms/strains		
Mus musculus C57BL/6J	Jackson Labs	Strain # 000664
For qRT-PCR primers used in this study see Table S1	see Table S1	see Table S1
Software and algorithms		
Prism v8.0	GraphPad	https://www.graphpad.com/scientific-software/prism/
MacVector v15.5.4	MacVector	https://macvector.com/downloads.html

Please cite this article in press as: Liou et al., Host cells subdivide nutrient niches into discrete biogeographical microhabitats for gut microbes, Cell Host & Microbe (2022), https://doi.org/10.1016/j.chom.2022.04.012

RESOURCE AVAILABILITY

Lead contact

Further information and requests for resources and reagents should be directed to and will be fulfilled by the Lead Contact, Andreas J. Bäumler (ajbaumler@ucdavis.edu).

Materials availability

All unique/stable reagents generated in this study are available from the Lead Contact without restriction.

Data and code availability

- The study did not create large datasets suited for deposition in a repository.
- The study did not generate or use custom code
- Any additional information required to reanalyze the data reported in this work paper is available from the Lead Contact upon request

EXPERIMENTAL MODEL AND SUBJECT DETAILS

Animal experiments

The Institutional Animal Care and Use Committee at the University of California, Davis, approved all animal experiments. Prior to transport, mice at Jackson were fed LabDiet 5K52 formulation (6% fat). Upon arrival, 8-10 week-old adult female mice from each cohort were randomly assigned into individually ventilated cages on one rack at a housing density of 3 to 4 animals per cage and allowed to acclimate in our vivarium for at least a week undisturbed. Feed was switched to irradiated TEKLAD GLOBAL 18% protein rodent diet 2918 (Envigo), which was also used for in-house breeding of *lys-EGFP-ki* mice, *Pparg*$^{fl/fl}$*Villin*$^{cre/-}$ mice and *Pparg*$^{fl/fl}$*Villin*$^{-/-}$ mice. Clean (but not sterile) paper towels were utilized for fecal sample collections and 70% ethanol was used to disinfect surfaces and gloves between groups.

For pre-treatment with streptomycin and infection with *E. coli* or *S.* Typhimurium strains or strain mixtures, *lys-EGFP-ki* mice (bred in house), bone marrow chimera mice (see below), wild-type (C57BL/6J) mice (Jackson Laboratories, Bar Harbor, ME) or *Nos2*-deficient (B6.129P2-*Nos2*^{tm1Lau}/J) mice (Jackson Laboratories, Bar Harbor, ME) were given streptomycin at 20 mg/mouse in 0.1 mL sterile water intragastrically 24 hours prior to inoculation with bacteria. In competition experiments, a 1:1 ratio of competing strains at a final concentration of 1×10^9 CFU/mouse in 0.1 mL LB broth was given intragastrically. In coinfection experiments, *S.* Typhimurium wild type or *invA spiB* mutant was given one day after streptomycin treatment, followed by inoculation with a 1:1 ratio of competing *E. coli* strains at a final concentration of 1×10^9 CFU/mouse in 0.1 mL LB broth intragastrically one day after *S.* Typhimurium infection. In single infections, 1×10^9 CFU/mouse of a single strain in 0.1 mL LB broth was given intragastrically.

For determining the effect *E. coli* have on colonization resistance against *S.* Typhimurium, mice (Jackson Laboratories, Bar Harbor, ME) were given streptomycin at 20 mg/mouse in 0.1 mL sterile water intragastrically 24 hours prior to inoculation with bacteria. Mice were inoculated intragstrically with *E. coli* strains (1×10^9 CFU/mouse in 0.1 ml LB) or 0.1 mL sterile LB broth (mock) one day after streptomycin treatment. Two days later mice were challenged with a 1:1 ratio of competing *S.* Typhimurium strains at a final concentration of 1×10^7 CFU/mouse in 0.1 mL LB broth intragastrically. Mice were euthanized 4 days after *S.* Typhimurium infection.

After euthanasia cecal or colonic tissue collected for histopathology was fixed in 10% buffered formalin phosphate overnight, whereas cecal tip sections for murine RNA analysis were flash frozen and stored at −80°C. Cecal contents were stored in phosphate-buffered saline (PBS) on ice. CFU counts were determined by plating serial 10-fold dilutions of the inoculum or colon content on selective medium. Plates were incubated overnight at 37°C under atmospheric oxygen conditions. For competitive infections, the output ratio of recovered bacteria strains was divided by the input ratio of the inoculum to determine the competitive index.

To generate bone marrow chimeras, recipients were subjected to lethal irradiation of 1000rad one day prior to bone marrow transfer of $5x10^6$ cells by intravenous injection. Mice were kept on antibiotics for 6 weeks following irradiation by diluting 5mL of sulfatrim pediatric suspension (Pharmaceutical Associates) containing 200mg sulfamethoxazole and 40mg trimethoprim into 250mL of water in water bottles.

Successful chimera generation was confirmed by flow cytometry on peripheral blood at 7-8 weeks post-donor cell injection. Approximately 50 ul of blood per mouse was collected from the facial vein into a sodium heparin-coated tube and placed immediately on ice until processing. After euthanasia, spleens were collected in DPBS and placed on ice until processing. Ceca were removed, fileted longitudinally, contents were gently removed by scraping with the blunt end of scissors. The cleaned cecal tissue was stored in RPMI on ice until processing. Single cell suspensions from the spleen and intestinal lamina propria were prepared as described below for analysis by flow cytometry.

Bacterial strains and culture conditions

The *E. coli* and *S.* Typhimurium strains used in this study are listed in Table S1. Bacteria were cultured routinely in Luria-Bertani (LB) broth (BD Biosciences #244620) or on LB plates unless otherwise indicated. For animal experiments, bacterial cultures were grown overnight at 37°C in LB broth under aerobic (atmospheric oxygen) conditions. 10ml of overnight culture were spun down and pelleted

at 4°C, then resuspended to a final concentration of $1x10^{10}$ CFU/ml in fresh media. Antibiotics were used at the following concentrations when required: carbenicillin (Carb), 0.1 mg/ml; chloramphenicol (Cm), 0.015mg/ml; kanamycin (Kan), 0.1 mg/ml; tetracycline (Tet), 0.02 mg/ml; spectinomycin (Spec), 0.1 mg/ml.

METHOD DETAILS

Construction of *E. coli* mutants

To generate *E. coli ΔnapA* and *ΔnarZ* mutants, respectively, plasmid pSW224 and pSW237 were transformed into *E. coli* S17-1 λ*pir* and conjugated into *E. coli* Nissle1917 carrying the temperature-sensitive plasmid pSW172 for counter selection. Conjugation was performed at 30°C and exconjugants in which the suicide plasmid had integrated into the chromosome were recovered on LB plates containing carbenicilin and chloramphenicol. Subsequent sucrose selection was performed on sucrose plates (5% sucrose, 8 g/L nutrient broth base, 15 g/L agar) to select for a second crossover events. PCR was performed to detect events that lead to the unmarked deletion of the *napA* or *narZ* genes, respectively. Plasmid pSW172 was then cured by cultivating bacteria at 37°C.

To construct a *fliC::tet* mutation in *E. coli*, primers were designed to overlap the 70 flanking base pairs on both ends of the *E. coli fliC* gene and 20 base pairs of the *tetRA* cassette from pSPN61. PCR was used to amplify the fragment with NEBuilder HiFi DNA Assembly Master Mix (NEB), run on an agarose gel, and gel purified via the Zymoclean Gel DNA Recovery kit (Zymo Research). The *fliC*::*tetRA* PCR product was desalted via drop dialysis using nitrocellulose membrane filters (Millipore), and subsequently DpnI (NEB) treated. The *E. coli* Nissle 1917 and *E. coli ΔnapAΔnarGΔnarZ* mutant (SW930) were electroporated with the temperature sensitive inducible lambda red recombinase plasmid pKD46 in which the ampicillin cassette has been replaced with a spectinomycin cassette. Nissle 1917(pKD46) and SW930(pKD46) were grown overnight at 30°C, 300μl were subcultured into 30ml of fresh media with spectinomycin at 30°C the next morning until OD_{600}=0.2, and the plasmid recombinase was induced with 10 mM arabinose. Nissle 1917(pKD46) and SW930(pKD46) was further grown at 30°C until OD_{600}=0.6, then spun down and washed with cold distilled water, and the *fliC*::*tetRA* PCR product introduced by electroporation. Mutants were selected via tetracycline resistance and confirmed for loss of pKD46 by loss of spectinomycin resistance. The mutations were verified via PCR screening.

For construction of the *tsr*::*tet* mutant we used the strategy described above, but primers were designed to overlap the 70 flanking base pairs on both ends of the *E. coli tsr* gene and 20 base pairs of the *tetRA* cassette from pSPN61.

Construction of *S. Typhimurium* mutants

To construct a *narZ*::Cm mutation in *S.* Typhimurium, primers were designed that overlapped the 70 flanking base pairs on both ends of the *S.* Typhimurium *narZ* gene and 20 base pairs of the chloramphenicol cassette from pKD3. PCR was used to amplify the fragment with NEBuilder HiFi DNA Assembly Master Mix (NEB), run on an agarose gel, and gel purified via the Zymoclean Gel DNA Recovery kit (Zymo Research). The *narZ*::Cm PCR product was desalted via drop dialysis using nitrocellulose membrane filters (Millipore), and subsequently DpnI (NEB) treated. *S.* Typhimurium strain IR715 was electroporated with the temperature sensitive inducible lambda red recombinase plasmid pKD46 in which the ampicillin cassette has been replaced with a spectinomycin cassette. IR715(pKD46) was grown aerobically in media with spectinomycin overnight at 30°C, 300μl were subcultured into 30ml of fresh media with spectinomycin at 30°C the next morning until OD_{600}=0.2, and the plasmid recombinase was induced with 10 mM arabinose. The induced IR715(pKD46) was further grown at 30°C until OD=0.6-0.8, then spun down and washed with cold distilled water, and the *narZ*::Cm PCR product introduced by electroporation. Mutants were selected via tetracycline resistance and confirmed for loss of pKD46 by loss of spectinomycin resistance. The insertion in *narZ* was verified via PCR screening and then transduced (P22, see below) into *S.* Typhimurium strain IR715, to generate strain ML96.

A *S.* Typhimurium *tsr*::*tetRA* mutant was constructed using the strategy described above, but primers were designed to overlap the 70 flanking base pairs on both ends of the *S.* Typhimurium *tsr* gene and 20 base pairs of the *tetRA* cassette from pSPN61. The mutation were verified via PCR screening.

P22 lysates (see below) of CAL34, CAL27, ML96 were prepared and transduced into *S.* Typhimurium strains IR715 (wild type), SPN487 (*invA spiB* mutant), and ML162 (*tsr* mutant) to generate a *napA*::Kan^R *narZ*::Cm^R *narG*::pCAL5 mutant, a *ΔinvA ΔspiB napA*::Kan^R *narZ*::Cm^R *narG*::pCAL5 mutant, and a *tsr*::tet^R *napA*::Kan^R *narZ*::Cm^R *narG*::pCAL5 mutant, respectively.

P22 lysates (see below) of QW111 and SM19 were prepared and transduced into *S.* Typhimurium strains SPN487 (*invA spiB* mutant) to generate a *ΔinvA ΔspiB mcpB*::Kan^R *mcpC*::Cm^R mutant, termed ML211. P22 lysate of CAL27 was then transduced into ML211 and ML108 (IR715 *ΔinvA ΔspiB phoN*:: Kan^R) to generate a *ΔinvA ΔspiB mcpB*::Kan^R *mcpC*::Cm^R *narG*::pCAL5 mutant, termed ML212, and a *ΔinvA ΔspiB phoN*:: Kan^R *narG*::pCAL5 mutant, termed ML215.

Plasmid pSPN29 was transformed into *E. coli* S17-1 λ*pir* and conjugated into *S.* Typhimurium strain CAL50 using sucrose selection to select for double cross-over as described above to construct a *ΔfliC narG*::pCAL5 *ΔnarZ ΔnapA* mutant, named ML53. A P22 lysate (see below) of an *S.* Typhimurium *fljB5001*::Mu*d*Cm mutant (SPN287) was transduced into ML53 to create a *ΔfliC fljB*::Mu*d*Cm *narG::pCAL5 ΔnarZ ΔnapA* mutant termed ML61.

Phage transduction

To generate S. Typhimurium phage lysates, we incubated 1 ml of an overnight culture of the strain of interest with 4 ml of P22 broth (LB broth supplemented with E minimal medium, 0.2% glucose, and 10^{10} to 10^{11} PFU/ml P22 *HT*-int) overnight at 37°C. Debris was removed by centrifugation at 10,000 × *g* for 5 min, and the phage-containing supernatant was mixed with chloroform (20% final

volume) and stored at 4°C. To transfer mutations between strains, diluted phage lysate prepared from the donor strain was incubated for 1 h at room temperature with an overnight culture of the recipient bacterial strain. The bacteria were then spread onto plates with the appropriate antibiotic. Resulting colonies were streaked onto Evans blue uranine agar plates (10 g/liter tryptone, 5 g/liter yeast extract, 5 g/liter NaCl, 2.5 g glucose, 15 g/liter Difco agar, 0.00125% Evans blue solution, 0.5% K_2HPO_4, 0.0025% sodium fluorescein) to select for non-lysogenic colonies. The sensitivity of the resulting strains to reinfection with P22 was determined by cross-streaking of the bacterial strain with P22 H5.

Nitrate measurements

Intestinal nitrate measurements were performed as described previously (Winter et al., 2013b). Briefly, mice were euthanized, and the intestine was removed and divided along its sagittal plane. The mucus layer was gently scraped from the tissue and homogenized in 200 μl PBS and then placed on ice. Samples were centrifuged at 5,000 × g for 10 min at 4°C to remove the remaining solid particles. The supernatant was then filter sterilized (0.2-μm Acrodisc syringe filter, Pall Life Sciences). Measurement of intestinal nitrate followed an adaptation of the Griess assay. In this assay, nitrate was first reduced to nitrite by combining 50 μl of each sample with 50 μl of Griess reagent 1 containing vanadium(III) chloride (0.5 M HCl, 0.2 mM VCl3, 1% sulfanilamide), and then the mixture was incubated at room temperature for 10 min. Next, 50 μl of Griess reagent 2 [0.1% (1-naphthyl)ethylenediamine dichloride] was added to each sample. Absorbance at 540 nm was measured immediately after the addition of Griess reagent 2 to detect any nitrite present in the samples. The samples were then incubated for 8 h at room temperature (to allow for reduction of nitrate to nitrite), and the absorbance at 540 nm was measured again. The initial absorbance (prior to reducing nitrate to nitrite) was subtracted from the absorbance after 8 h to determine nitrate concentrations in the cecal mucus layer. Samples were tested in duplicate, and all measurements were standardized to the initial sample weight. Nitrate concentrations were determined based on a standard curve derived from similarly treated dilutions of sodium nitrate.

Generation of bone marrow chimeras

To generate bone marrow chimeras, recipient C57BL/6-Ly5.1 mice (Jackson Laboratories, Bar Harbor, ME) were subjected to lethal irradiation of 1000rad one day prior to bone marrow transfer of $5x10^6$ cells from donor mice (C57BL6/J or B6.129P2-*Nos2*^{tm1Lau}/J mice from Jackson Laboratories, Bar Harbor, ME) by intravenous injection. Mice were kept on antibiotics for 6 weeks following irradiation by diluting 5mL of sulfatrim pediatric suspension (Pharmaceutical Associates) containing 200mg sulfamethoxazole and 40mg trimethoprim into 250mL of water in water bottles. Successful chimera generation was confirmed by flow cytometry on peripheral blood at 7-8 weeks post-donor cell injection. Approximately 50 μL of blood per mouse was collected from the facial vein into a sodium heparin-coated tube and placed immediately on ice until processing.

Flow cytometry and tissue processing

"Staining media" was prepared with mouse isotonic HEPES buffered balanced salt solution (840 ml/L of 1.68M NaCl, 21 ml/L of 1.68M KCL, 21 ml/L of 1.12M $CaCl_2$, 7 ml/L of 1.68M $MgSO_4$, 14 ml/L of 0.84M KH_2PO_4 + 0.56M K_2HPO_4, and 84 ml/L of 0.84M HEPES + 0.84M NaOH), 3.5% neonatal calf serum, and 1 mmol EDTA, pH 7.2 (Rothaeusler and Baumgarth, 2006).

To process the blood samples, staining media was used to transfer blood into a 15 ml Falcon tube, which was then spun at 500g x 5 mins and the supernatant removed. 1 ml ACK (Lonza Bioscience) was added to lyse red blood cells, samples were incubated at room temperature for 5 mins, then 4 ml staining media was added, the samples spun at 500g x 5 mins, and the supernatant was removed. Samples were then stained as described below with CD45.1-FITC (Biolegend) and CD45.2-PE (Biolegend).

Single cell suspensions of spleens were generated by grinding tissues between the frosted edges of two microscope slides, suspending in staining media, spinning at 500g x 5 min and removing supernatant, treating with ACK lysis buffer as described above, and filtered through a 50 μm nylon mesh. For collection of intraepithelial and lamina propria lymphocytes from the large intestines, intestines were opened longitudinally and stored in RPMI on ice until processing. Samples were washed in PBS, then diced, transferred in a C-tube (Miltenyi) with 300 units DNAse I (Roche) and 0.54 W units of Liberase (Sigma), then run on the gentleMACS (Miltyenyi) Brain 1.01 cycle twice. Samples were then incubated with rotation at 37°C for 35 mins and run on gentleMACS Brain 1.01 cycle until homogenized, filtered through a 50 μm nylon mesh, and washed as described above with staining media. Cells were counted using Trypan Blue to exclude dead cells. Cells were stained at a concentration of $6.25x10^5$ cells/25 μL using CD3-eFluor780 (eBiosciences), CD11b-Alexa700 (eBiosciences), CD11c-PerCP Cy55 (eBiosciences), CD45.1-FITC (Biolegend), CD45.2-PE (Biolegend), CD45R-PECy7 (eBiosciences), Ly6c-Pacblue (Biolegend), Ly6g-APC (Biolegend), and NK1.1-BV605 (BD).

Fc receptors were blocked using an unlabeled anti-CD16/32 antibody (Invitrogen) and stained with the indicated fluorochrome conjugates at previously determined optimal staining concentrations. Samples were washed with staining media between each step and maintained on ice, protected from light, throughout the staining process. Dead cells were identified using Live/Dead Fixable Aqua (Invitrogen). All samples were fixed with BD Cytofix fixation buffer for 30 minutes, then stored at 4°C until analysis. FACS analysis was performed on a 3-laser, 16-color LSRII (BD Bioscience). Data were analyzed using FlowJo software (FlowJo LLC).

RNA isolation and quantitative real-time PCR

Murine colon tissue samples were collected as described previously (Lopez et al., 2012). Samples were homogenized in TRI Reagent (Molecular Research Center, Inc.) using a Mini-Beadbeater (BioSpec Products) and RNA was isolated following the manufacturer's

protocol. RNA was eluted in DNAse buffer and contaminating DNA was removed using the DNA-free kit (Applied Biosystems), and RNA was stored at −80°C.RNA concentration and quality were measured spectrophotometrically using a Nandrop (ND-1000, Nanodrop Technologies). Isolated RNA from murine samples was reverse transcribed using random hexamers and MuLV reverse transcriptase (Applied Biosystems). Quantitative real-time PCR (qPCR) was performed using SYBR green PCR mix (Applied Biosystems) and the primer sets listed in Table S2 to a concentration of 0.25 mM. Delta delta Ct was used to calculate fold change between groups.

Histopathology

Colonic tissue was fixed in 10 % phosphate-buffered formalin and 5 μm sections of the tissue were stained with hematoxylin and eosin. Scoring of blinded tissue sections was performed by a veterinary pathologist based on the criteria listed in Table S3. Representative images were taken using an Olympus BX41 microscope.

Detection of myeloperoxidase

Cecal contents from mice were collected in PBS and stored on ice until processing. Larger particles were removed by centrifugation at 20,000 g for 5 min at 4°C and the supernatant stored at -20°C. Murine myeloperoxidase (R&D Systems, 10 DY3667) levels were determined by sandwich enzyme-linked immunosorbent assay (ELISA) in cecal content supernatant according to the manufacturer's instructions. A minimum of 4 biological replicates were used for each experimental group.

Fluorescence imaging

For imaging the murine colon, 10-15 mm segments of mid-colon were fixed with 4% PFA, dehydrated with 20% sucrose, frozen in Optimal Cutting Temperature (OCT) compound (Fisher HealthCare) and cut in transverse sections to a thickness of 7μm, and permeabilized with 0.2% Triton-X 100 before staining. For imaging the murine ceca, 5-10 mm segments of the cecal tip and processed as described above. *S.* Typhimurium cells were stained with a rabbit anti-Salmonella O12 serum (Becton-Dickson, 227791), *E. coli* cells were stained with a rabbit anti-*E. coli* O6 (Abcam, ab78824) and a goat anti-rabbit Alexafluor 647conjugate (Abcam, ab150079). LysM-EGFP cells were stained with a goat anti-GFP antibody (Abcam, ab6673) and a donkey anti-goat Alexa Fluor 488conjugate (Abcam, ab150129). Nuclei were stained with DAPI (ThermoFisher). Actin was stained using phalloidintetramethylrhodamine B isothiocyanate (Sigma Aldrich). Sections were mounted in Immu-Mount (Thermofisher).

Segmentation of immunofluorescence images

Segmentation and quantitative analysis of immunoflourescence images was performed using MATLAB. First, segmentation of the epithelial brush border was performed on actin immunofluorescence images to determine the apical epithelial surface. General segmentation of actin-rich regions was achieved via automated pixel intensity thresholding using the 'graythresh' function in MATLAB followed by removal of small (<15 μm^2) objects and morphological closing (mask dilation followed by erosion) using MATLAB's 'imclose' function to smooth mask edges. Masks of the brush border were isolated by manually identifying and removing the basement membrane from masks using the 'drawpolygon' and 'createMask' functions in MATLAB. Next, segmentation of bacterial colonization zones was performed on bacterial immunofluorescence images via automated pixel intensity thresholding using the 'graythresh' function in MATLAB, removal of small (<6 μm^2) objects, morphological closing to smooth mask edges, and mask dilation using a disk-shaped structuring element with a radius of 3 pixels (~1.8 μm). Regions of the bacterial masks that occurred behind the epithelial boundary were removed to ensure that artifacts from sample preparation did not affect quantitative measurements.

QUANTIFICATION AND STATISTICAL ANALYSIS

Quantification of bacterial distance from epithelium

We wanted to determine the distance between bacterial colonization zones and the epithelium while accounting for the non-uniform densities of bacteria within these zones. To this end, we generated a set of ''seed pixels'' within colonization zones to represent bacterial positions with a smaller number of discrete points, with local point densities determined by the local intensity of the bacterial immunofluorescence signal. We first generated contoured bacterial masks with four contour regions corresponding to different fluorescence intensity intervals. Immunofluorescence images were smoothed using a Gaussian filter of width 5 pixels (3.1 μm) to reduce pixel noise. Contoured regions were then determined using pixel intensity thresholding based on four intensity ranges ($0 \leq$ contour1 < 30, $30 \leq$ contour2 < 60, $60 \leq$ contour3 < 120, and contour4 ≥ 120). The ranges were chosen such that the number of pixels in each contour were similar, and ranges were kept constant across all images. The seed pixels in each contour were set using MATLAB's 'meshgrid' function to generate regularly spaced pixel grids and different pixel densities were achieved by adjusting the block size for each contour (block sizes were 1, 2, 3, or 4 pixels going from high-intensity to low-intensity contours). Finally, original bacterial masks were applied to the seed pixel contours to restrict seed pixels to the bacterial colonization zones. Distance values were calculated by measuring the distance between each seed pixel in the contoured bacterial masks and the closest pixel within corresponding epithelial masks. We did not use methods to determine whether the data met assumptions of the statistical approach.

Statistical analysis

Data for all experiments displayed as bar graphs represent the geometric mean and the geometric error of the mean. For experiments involving *Pparg*$^{fl/fl}$*Villin*$^{cre/-}$ mice, differences between experimental groups were determined using an unpaired, one-tailed Mann-Whitney test (for comparing two groups). For all other experiments, differences between experimental groups were determined using an unpaired, two-tailed Mann-Whitney test (for comparing two groups) or ANOVA followed by Fisher's LSD post hoc test (for comparison of more than two groups). A *P*-value of less than 0.05 was considered significant. We did not use methods to determine whether the data met assumptions of the statistical approach.